Title

Characterization of nitrogen-containing radical products from the photodissociation o f trimethylamine at 193 nm using photoionization detection

Journal

Journal of Chemical Physics, 113(8)

Author

Forde, N.R.

Publication Date

2000

LBNL-45219
Preprint

ERNEST ORLANDO LAWRENCE
BERKELEY NATIONAL LABORATORY

Characterization of Nitrogen-Containing Radical Products from the Photodissociation of Trimethylamine at 193 nm using Photoionization

Nancy R. Forde, Laurie J. Butler, Branko Ruscic,
Osman Sorkhabi, Fei Qi, and Arthur Suits

Chemical Sciences Division

January 2000

Submitted to
Journal of Chemical Physics

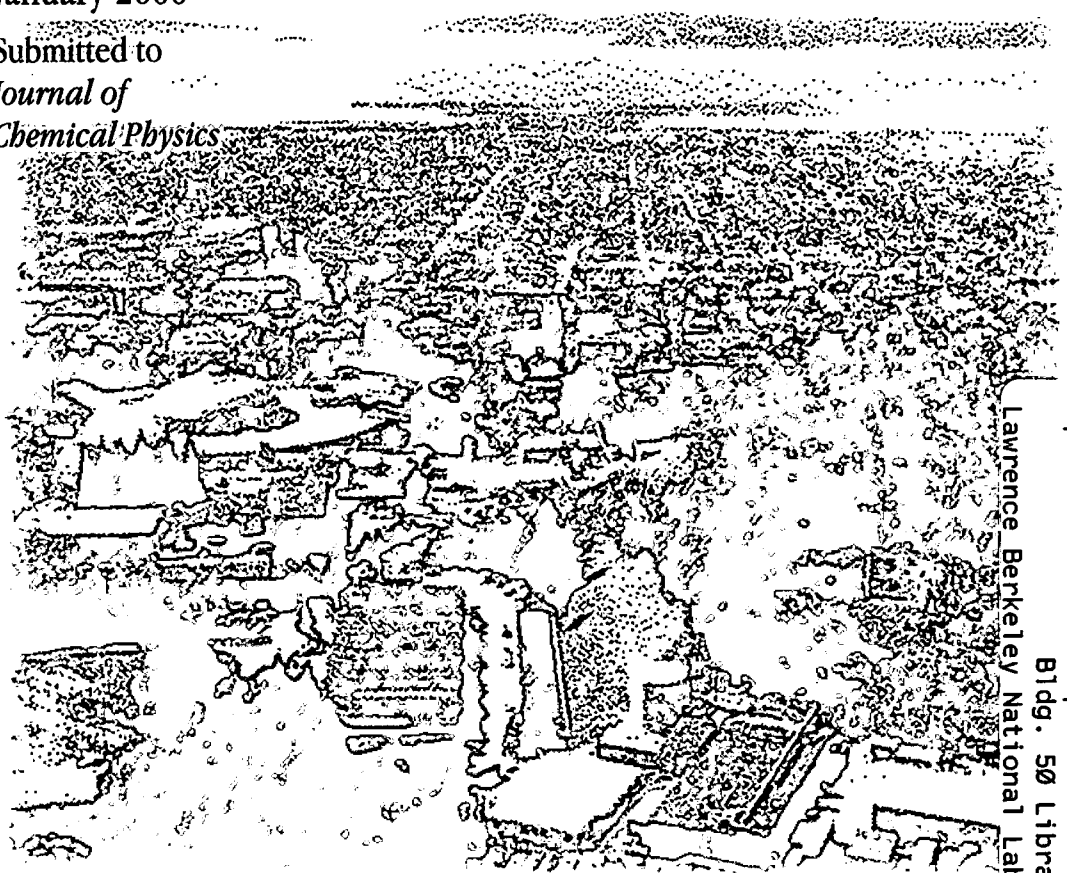

DISCLAIMER

LBNL-45219

Characterization of Nitrogen-Containing Radical Products from the Photodissociation of Trimethylamine at 193 nm using Photoionization

Nancy R. Forde,[1] Laurie J. Butler,[1] Branko Ruscic,[2]
Osman Sorkhabi,[3] Fei Qi,[3] and Arthur Suits[3]

[1]The James Franck Institute and Department of Chemistry
University of Chicago
Chicago, IL 60637

[2]Chemistry Division
Argonne National Laboratory
Argonne, IL 60439

[3]Chemical Sciences Division
Ernest Orlando Lawrence Berkeley National Laboratory
University of California
Berkeley, California 94720

January 2000

This work was supported by the Director, Office of Science, Office of Basic Energy Sciences, Chemical Sciences Division, of the U.S. Department of Energy under Contract Nos. DE-FG02-92ER14305 and DE-AC03-76SF00098.

Characterization of Nitrogen-Containing Radical Products from the Photodissociation of Trimethylamine at 193 nm using Photoionization Detection

Nancy R. Forde and Laurie J. Butler
The James Franck Institute and Department of Chemistry
University of Chicago, Chicago, IL 60637

Branko Ruscic
Chemistry Division, Argonne National Laboratory, Argonne, IL 60439

Osman Sorkhabi, Fei Qi and Arthur Suits
Chemical Sciences Division, Lawrence Berkeley National Laboratory, Berkeley, CA 94720

Abstract

Both the neutral and ionized forms of $N(CH_3)_2$ primary products of trimethylamine photodissociation at 193 nm undergo complex secondary dissociation processes, including unusual ionization dynamics. By combining photoionization detection with supporting G3 theoretical calculations, this study seeks to identify the primary and secondary neutral products formed in the photodissociation. $N(CH_3)_2$ primary products with very little internal energy show an experimentally observed ionization onset of 9.1±0.2 eV, but do not appear at the parent ion (*m/e*=44). Instead, the parent ion is unstable and easily fragments to *m/e*=42, where signal is observed. $N(CH_3)_2$ radicals with higher internal energies undergo H-atom loss from the neutral to give CH_2NCH_3, which has an observed ionization onset at parent (*m/e*=43) of <9.3 eV. At slightly higher ionization energies, these secondary products also appear at *m/e*=42 (where their

appearance energy is roughly 9.8-9.9 eV, uncorrected for internal energy). Finally, $N(CH_3)_2$ radicals with the highest internal energy in this study appear to undergo H_2 loss as neutrals, giving rise to a species whose parent ion has *m/e*=42. The ionization onset of this species at *m/e*=42 is found to be in the range of 9.5-9.6 eV.

I. Introduction

We recently reported the results of the photodissociation reactions of trimethylamine ($N(CH_3)_3$) following 193 nm excitation.[1] In analyzing the resulting dissociation pathways, we discovered that little is known about the energetics and ionization characteristics of methylated nitrogen-containing radicals. These radicals were of interest to us both as products of the photodissociation reactions of trimethylamine[1] and dimethylformamide[2,3] at 193 nm, and also as possible participants in combustion reactions. The experiments outlined in this paper seek to characterize the methylated nitrogen-containing products of the photodissociation of trimethylamine at 193 nm, by analyzing both their energetics and ionization properties.

The earlier photodissociation experiments on trimethylamine described in Reference 1 used the technique of universal detection.[4] This detection method involves electron impact ionization of neutral molecules and is powerful because of its universality: the 200 eV electrons that bombard neutral radicals and molecules are well above the ionization potential of all neutral species, ionizing

roughly 10^{-4} of each species. The disadvantage of using such high-energy electrons is the large internal energy of the nascent ions, which undergo dissociative ionization (fragmentation or "cracking") prior to detection. The experimental signal is then detected at mass/charge ratios corresponding to ionic fragments. For example, in the work on trimethylamine, the neutral CH_2NCH_3 secondary product was found to appear upon electron impact ionization at *m/e*=43, 42 and 15.[1] To unambiguously identify the neutral precursors, one normally relies on momentum-matching the signal from the two neutral fragments, but if one fragment can undergo secondary dissociation via H-atom loss, the velocity of the neutral fragment may not be significantly altered, and the secondary neutral reaction can be missed. Photoionization detection in this study identified the secondary product formed from H-atom elimination from $N(CH_3)_2$).

This study employs tunable photoionization detection of the primary and secondary neutral photofragments. Tunable photoionization, at least in principle, permits sensitive detection of reaction products just above their threshold for ionization, which, by reducing the excess internal energy of the parent ions, eliminates or significantly reduces the dissociative ionization channels. At the same time, the absence of a hot filament required for electron impact ionization greatly diminishes background counts. The photoionization approach was of particular interest for characterizing the outcome of the primary

$N(CH_3)_2$ radical products of the photodissociation of trimethylamine.[1] The lack of ion signal at the parent mass/charge ratio (*m/e*=44) of $N(CH_3)_2$ in previous experiments[1-3] implied that the $N(CH_3)_2^+$ ion is unstable when formed by 200 eV electron impact ionization. By utilizing the much softer photoionization conditions available at the ALS, we hoped to be able to observe parent ion signal at *m/e*=44 and determine its onset. We did not, instead finding that even near threshold, $CH_3NCH_3^+$ is unstable to H_2 loss from the ion. These results and others are described within.

Nitrogen-methyl bond fission was the only primary photodissociation pathway identified following 193 nm excitation of trimethylamine.[1] The primary $N(CH_3)_2$ radical products were found to exhibit distinct ionization characteristics depending on their internal energy (given by the 193 nm photon energy minus the N-CH_3 bond energy and observed translational energy). This suggests the existence of additional channels, possibly proceeding through secondary dissociation of the neutral species and/or competitive fission to electronically excited $N(CH_3)_2$ ($\tilde{A}^2A_1$) radicals. Several possibilities can be considered:

$$N(CH_3)_3 + 193\text{ nm} \rightarrow N(CH_3)_2\,(\tilde{X}^2B_1) + CH_3$$
$$\rightarrow CH_3N{=}CH_2 + H + CH_3$$
$$\rightarrow NC_2H_4 + H_2 + CH_3$$
$$\rightarrow N(CH_3)_2\,(\tilde{A}^2A_1) + CH_3$$

In order to identify which of these channels contribute to the dissociation dynamics, one needs to understand the properties of the possible reaction products. Unfortunately, there have been very few studies on these nitrogen-containing species, particularly the radicals $N(CH_3)_2$ and NC_2H_4. In the following paragraph, we summarize what is known about each species.

Values for the heat of formation of the $N(CH_3)_2$ radical found in the literature range from 29.3±2 kcal/mol to 39 kcal/mol (see Table I).[5-20] Determinations of its ionization energy fall into an even wider range, 9–10 eV, with one much lower value.[5,8,21-23] Additionally, very little is known of the electronically excited states of this radical. Third order H^v calculations found $N(CH_3)_2$ ($\tilde{A}^2A_1$) to lie 1.59 eV higher than $N(CH_3)_2$ ($\tilde{X}^2B_1$).[3,24] This adiabatic value was determined from geometries optimized at a lower level of theory, and so should be taken only as an estimate to the true minimum energy separation. The stable secondary product $H_2C{=}NCH_3$ has a calculated heat of formation is 11±2 kcal/mol (see Table I), and its ionization energy has been found by various studies to range from 9.3 eV to 10.0 eV, where the larger values correspond to the vertical ionization energy.[5] Neutral species of formula NC_2H_4 have not been well characterized. Various possibilities exist for the structure of these species, including the linear $HCNCH_3$ and H_2CNCH_2 forms.

This study provides a characterization of both the $N(CH_3)_2$ radical and its secondary neutral and ionic dissociation channels by using the photodissociation

of trimethylamine at 193 nm as a primary radical source. The amount of internal energy in the primary $N(CH_3)_2$ products can be determined by analyzing the amount of energy disposed to relative product translation of the $N(CH_3)_2 + CH_3$ products. These energies, together with the photoionization detection schemes available at the ALS, allow us to obtain experimental limits on the enthalpies of formation and ionization energies of the resulting nitrogen-containing radicals and closed-shell species. By combining these results with theoretical calculations, we have characterized the secondary dissociation channels of the $N(CH_3)_2$ radical photoproduct, providing a deeper understanding of the complicated dynamics at play in these nitrogen-containing systems.

II. Experimental Details

These experiments studied the photodissociation products of trimethylamine at 193 nm by detecting the neutral photofragment recoil distributions with a crossed laser-molecular beam apparatus.[25] After photodissociation with a pulsed excimer laser, neutral products scattered from the crossing point of the laser and the molecular beam with velocities determined by the vector sum of the molecular beam velocity and the recoil velocity imparted during dissociation. Dissociation products were detected following photoionization and mass selection as a function of their times of flight (TOF) with respect to the dissociating laser pulse. Forward convolution fitting of the TOF spectrum (taking into account the ion flight time) determines the

distribution of energies released to relative product translation in the dissociation. The plane defined by the molecular beam and the detector axis is perpendicular to the direction of laser propagation, and molecular beam source angles are given here with respect to the detector axis.

The crossed laser-molecular beam apparatus employed in these experiments is described in detail in Reference 25. It has a rotating source region with two sources: a pulsed valve and a nozzle for continuous beam expansion. We used a continuous beam to verify that the signal following photoionization at the Advanced Light Source arose from the same primary dissociation events as earlier experiments performed at the University of Chicago.[1] We then switched to the pulsed valve for the experiments described in this paper, as the pulsed expansion resulted in much stronger signal while still avoiding significant contributions from clusters. Because of this, we were able to record data at source angles up to 50• with respect to the detector axis, important for accurate fitting of translational energy distributions to the quickly recoiling methyl products.

Tunable photons employed for the product detection via photoionization were produced when the ALS electron beam passes through a U10 undulator (bandwidth at FWHM=0.5 eV).[26,27] Various filtering methods were used to eliminate higher harmonics of the selected energy. Most of the power in the higher harmonics is absorbed by the mirrors used to direct light from the

undulator towards the endstation, by strongly attenuating photon energies above 70 eV and virtually eliminating those above 400 eV.[28] The remaining higher harmonic radiation was removed with a differentially pumped, windowless gas filter filled with argon.[28] Under these conditions, the higher harmonics are suppressed by a factor of 10^4, while attenuation of the fundamental is less than 5%.[28] Finally, for photon energies less than 11 eV, a MgF_2 filter was placed in the beam, virtually eliminating all photon flux above 11 eV but decreasing the intensity of the desired lower energy light by 35%.[26,27] Unless otherwise noted, the experiments described in this paper used probe photon energy of 10.5 eV with the MgF_2 window in place, resulting in a net photon flux of $8x10^{15}$ photons/second (with a new electron fill and 400 mA ring current).

A 5% mixture of trimethylamine ($N(CH_3)_3$) in helium (obtained from Matheson Gas Products) was expanded from the pulsed valve source (nozzle diameter = 1 mm), with a stagnation pressure of 500 Torr. The low percentage gas mixture of trimethylamine was used to prevent formation of clusters (a problem well addressed in the literature[29,30]). A scan of the mass spectrum in the range from monomer to dimer mass/charge ratio under typical experimental conditions revealed no contributions from species of higher mass than monomer. The intensity of the parent $N(CH_3)_3^+$ ion signal was, however, strongly dependent on ionization energy through the range of 9-12.7 eV. The ionization potential of

trimethylamine is 7.85 eV,[5] and for probe photon energies below 10 eV, the signal at parent (*m/e*=59) was much stronger than the signal at *m/e*=58. At higher ionization energies, however, the parent peak diminished in intensity as dissociative ionization became competitive, such that at 12.7 eV, the peak at *m/e*=58 was much more intense than the parent peak. Determination of the beam parameters, accomplished via hole-burning at the parent ion (*m/e*=59), used either 10 eV or 10.5 eV photons to reduce dissociative ionization. The mean peak beam velocity was 1.30×10^5 cm/s with a full width at half-maximum (FWHM) of 35%.

In the experiments described here, we have measured the signal for several parent and daughter ions of the neutral photoproducts at various angles of the molecular beam with respect to the detector axis: at *m/e* = 43 (10•, 11 eV; 30•, 11eV), 42 (30•, 10 eV; 30•, 10.5 eV; 30•, 11 eV) and 15 (30•, 10.5 eV; 50•, 10.5 eV). No discernible signal was observed at *m/e* = 57 (10•, 10.5 eV), 30 (10•, 10.5 eV), 29 (10•, 10.5 eV), 17 (30•, 10.5 eV) or 16 (10•, 13.5 eV). The quadrupole was adjusted to approximately 0.4 amu resolution (FWHM).

In addition, a very small signal was observed at *m/e*=44 (10•, 10 eV; 10•, 10.5 eV; 30•, 10.5 eV). In order to determine the source of this signal, photofragment TOF spectra were collected at 0.2 amu intervals from *m/e*=42.0 to 44.0 (30•, 10.5 eV). Because this signal is observed off the molecular beam (center-of-mass) velocity axis, it arises from photoproducts. One can determine

the source of this signal by integrating the area under the photofragment TOF spectrum as a function of the mass/charge ratio of the ions passing through the quadrupole mass filter. The resulting integrated peak intensities (see Figure 1) show that, while photoproducts appear at *m/e*=42 and 43 (with clear separation of the masses by the quadrupole), no *m/e*=44 can be discerned above the very small high-mass wing of *m/e*=43. In addition, the photoionization curves constructed from data collected nominally at *m/e*=44 appeared identical to those obtained for the *m/e*=43 signal. This places an upper limit on the possible intensity of the signal at *m/e*=44 to $<10^{-3}$ of the intensity at *m/e*=43.

We determined the photoionization yields for the photoproduct signal at *m/e*=42 and 43 by recording TOF spectra at each mass. The spectra were collected at 0.2 eV increments of the nominal photon energy from 8.7-10.7 eV (*m/e*=42) and from 8.5-10.7 eV (*m/e*=43), for 50,000 laser shots each with a 30• angle between the molecular beam and detector axes. The MgF_2 window was in place for all of these scans, and the laser power was held constant at 55 mJ/pulse. The integrated peak area for each species was corrected for drift in the probe photon flux and was plotted as a function of photoionization energy.

A power study of the observed TOF signal was the most direct way to ensure that the electronic transition of trimethylamine was not saturated. (The ArF excimer transition provided the 193 nm light.) We conducted a power study of the signal at *m/e*=42 with laser powers ranging from 10 mJ/pulse to 60

mJ/pulse, resulting in attenuated powers of roughly 80% in the interaction region, a cross-sectional area of 1x3 mm^2. It revealed no change to the fast edge of the TOF spectrum, and so the experiments described in this chapter were run with a laser power of between 50-60 mJ/pulse, at 100 Hz repetition rates.

III. Theoretical Methodology

Supporting calculations were performed using the Gaussian 98 package of programs.[31] The intent of these calculations was not to perform an exhaustive theoretical study of species corresponding to NC_nH_m and $NC_nH_m^+$, but rather to provide insight into the possible dissociation and ionization channels of relevance to these experiments. As shown previously,[7,30,32-39] the potential energy surfaces of these species (particularly in the case of ions) are quite complex and exhibit a considerable number of isomers and conformers, resulting in a large number of minima and saddle points. Rather than performing a thorough examination of the potential energy surfaces, the goal here was to examine a select subset of the NC_nH_m and $NC_nH_m^+$ species. It was hoped that these calculations would provide sufficient guidance on plausible values for bond dissociation energies, ionization energies and fragment appearance energies corresponding to dissociative ionization to enable determination of the ionic and neutral species formed in the present experiments.

Calculations leading to thermochemical quantities presented in Tables II - V were performed at the G3 level of theory,[40] which is the latest in the series of

Gaussian-n theories, and has been shown to achieve higher accuracy than its G2 predecessor.[40-42] Using the G2/97 test set, the reported overall average absolute deviation between experiment and the G3 results is 1.02 kcal/mol, actually corresponding to a standard deviation σ = 1.47 kcal/mol. Hence, at least for the species considered in the present work, one expects the G3 calculated results to be within ±3 kcal/mol of the true value (where the error bar has been arrived at by using 2σ to estimate the ~95% confidence level, as customarily reported by experimentalists).

Just as the earlier Gn calculations, the unmodified G3 sequence (which was used here) starts by optimizing the initial geometry and calculating vibrational frequencies at the HF/6-31G(d) level, followed by re-optimizing the geometry at the MP2(Full)/ 6-31G(d) level. The MP2 geometry is then used to perform the remaining calculations, which in the case of G3 are QCISD(T)/6-31G(d), MP4/6-31+G(d), MP4/6-31G(2df,p), and MP2(Full)/G3Large. These lead to an estimate of the total electronic energy that is effectively at the QCISD(T,full)/G3Large level. The final G3 total electronic energy is then obtained by including small empirical "higher level" corrections.

Within the G3 procedure, the role of the initial HF calculations is simply to provide the first step in the geometry optimization and yield vibrational frequencies that are used to estimate the zero-point vibrational energy. However, these frequencies are also used as an indicator of whether the proposed geometry

corresponds to a true local minimum or a saddle point on the potential energy surface. Of the various structures examined here, ~1/3 appeared to belong to local minima, while ~2/3 corresponded to first or second order saddle points at the HF level. However, at least in principle, the subsequent MP2 optimization may drift away from the initial HF geometry, resulting in a G3 calculation for a different conformer or isomer. In addition, a geometry that corresponds to a stable minimum at the HF level, may correspond to a saddle point at the MP2 level and vice versa. In order to avoid such surprises, the majority of structures, whether corresponding to true minima or saddle points with one or more imaginary frequencies at the HF level, were rechecked by performing a geometry optimization and computation of frequencies at the B3LYP/6-311G(d,p) level of theory.[43-45] In general, the additional B3LYP calculations confirmed the G3 findings based on the HF and MP2 optimizations. With one exception, only species corresponding to true minima both at the HF/6-31G(d) and B3LYP/6-311G** levels are reported in Tables II-III.

IV. Results and Analysis

The photofragment TOF spectra from these experiments are consistent with the results of earlier experiments, showing N-CH_3 bond fission to be the dominant (perhaps only) primary dissociation event following 193 nm excitation.[1] The photofragment TOF spectra at *m/e*=43, 42 and 15 (shown in Figures 2-4) were fit by recoil translational energy distributions, $P(E_T)$'s (shown

in Figure 5), corresponding to primary N-CH_3 bond fission. The assignment of these distinct channels to the processes

$$N(CH_3)_3 + 193\ nm \rightarrow CH_3 + N(CH_3)_2\ (\tilde{X}^2B_1) \quad (1)$$

$$\rightarrow CH_3 + N(CH_3)_2^* \rightarrow CH_3 + H_2C{=}NCH_3 + H \quad (2)$$

is shown in the following sections. Additionally, here we suggest that the slow, unfit signal at *m/e*=42 (Figure 3) is an NC_2H_4 product arising from secondary dissociation:[1]

$$N(CH_3)_3 + 193\ nm \rightarrow CH_3 + N(CH_3)_2^{\dagger} \rightarrow CH_3 + NC_2H_4 + H_2. \quad (3)$$

Photoion yield curves obtained by integrating photofragment TOF spectra at *m/e*=43 and 42 (the only mass/charge ratios at which nitrogen-containing reaction products were observed in the present experiments) were used to characterize the products and are analyzed in the following sections. The results show that reactions (1)-(3) produce species with distinct photoionization characteristics. Because the reaction products can be identified by kinetic energy release, we have determined that following 10.5 eV photoionization, the nitrogen-containing products of reactions (1) and (3) appear at *m/e*=42, while the nitrogen-containing product of reaction (2) appears at both *m/e*=43 and *m/e*=42. Additionally, each component of the TOF spectrum at *m/e*=42 was found to have a distinct photoionization curve. Thus, each of the three distributions arises from a different neutral precursor.

IVA. Species appearing at m/e=43: CH_2NCH_3

Figure 2 shows a TOF spectrum recorded at a 30• source angle, at *m/e*=43 and with 10.5 eV probe photon energy. The translational energy distribution ($P(E_T)$) used to fit this spectrum (attributed to reaction (2)) is shown as the slower one in Figure 5. The $P(E_T)$'s given in Figure 5 are identical to those used previously to fit the 200 eV electron impact (EI) data.[1] (The faster distribution attributed to reaction 1 could also contribute to the signal at *m/e*=43, but would be most likely responsible for only a minor fraction of the total signal.) Thus, the translational energy release for reaction (2) is independent of the technique used for ionization (electron impact or photoionization), as should be the case.

The photoionization efficiency curve shown in Figure 6 exhibits a prominent ascent, perhaps starting to level off at the high energy side, and preceded by a rounded "tail" extending to lower energy. Although the photon resolution in these experiments is relatively low, the shape of the curve can be interpreted as representing the parent ionization of a species with a relatively broad Franck-Condon envelope, where the observed photoion spectral shape roughly corresponds to an integral over this envelope. The tail region hides unresolved initial (low) Franck-Condon factors, which, as the photon energy increases, build up and attain maximum probability in the region of steepest slope, finally leveling off when the Franck-Condon envelope is exhausted. Hence, the middle of the ascent region corresponds to the vertical ionization

energy. If indeed the point at highest energy indicates a leveling off of the photoion signal, then the vertical ionization energy of the species that gives rise to the TOF spectrum at *m/e*=43 should be close to ~10.0 eV.

Ideally, the signal onset at the low-energy end should correspond to the adiabatic ionization energy. However, the tail region is rendered complex by several factors, which tend to work in opposite directions: very low Franck-Condon factors tend to push the experimentally measurable onset to energies higher than the true adiabatic ionization energy, while low photon resolution and hot bands (arising from neutrals that are internally excited in the Franck-Condon active symmetric vibrational mode) tend to push the apparent onset toward lower energy. Selecting a point just before the more pronounced section of the ascent, such as ~9.3 eV, should produce a relatively "safe" upper limit to the adiabatic ionization energy. The true adiabatic onset is expected to be in the "tail" region, at a lower energy and difficult to pinpoint more accurately.

It should be noted that, besides parent ionization of NC_2H_5, the ion yield at *m/e*=43 could have a small contribution from photodissociative ionization of $N(CH_3)_2$ leading to $NC_2H_5^+$ fragment ions (implying that the $P(E_T)$ assigned to reaction (2) also includes contributions from reaction (1)). The appearance energies for $NC_2H_5^+$ ions from an $N(CH_3)_2$ neutral precursor are 10.6 and 11.3 eV, respectively (see Table IV), assuming that the ions formed are either CH_3-N-CH_2^+, $^2A'$ (C_s) or H_2C-NH-CH_2^+, $^2A'$ (C_s ring). , These values certainly cannot easily

explain the bulk of the photoion yield spectrum in Figure 6, but of course, there may be other as yet unidentified, more stable $NC_2H_5^+$ ions, leading to lower values for the fragment appearance energies. While fragmentation into one of these potentially more stable ions would require rearrangement, such processes are notorious for being very facile on the ionic potential energy surface, and, in, most cases the most stable isomer of the fragment ion can be relatively easily reached by photodissociative ionization. However, the kinetic energy analysis has shown that the contribution from photodissociative ionization of neutral $N(CH_3)_2$ to *m/e*=43 is minor. (At best, there is a very small portion of the fast edge of the TOF spectrum at *m/e*=43 that could be fit using reaction (1).) Furthermore, it would appear (*vide infra*) that the primary fragment ion generated by photodissociative ionization of $N(CH_3)_2$ is $NC_2H_4^+$, and appears at *m/e*=42.

If indeed the bulk of the TOF signal at *m/e*=43 originates from parent ionization, then the neutral species in question has a composition NC_2H_5 with a vertical ionization energy of ~10.0 eV and an adiabatic ionization energy of <9.3 eV. The simplest secondary dissociation process to produce NC_2H_5 from the primary $N(CH_3)_2$ product is straightforward C-H bond cleavage, leading to a CH_3-N=CH_2 structure. In agreement with this, we see in Table IV that the adiabatic ionization energy $IE_a(CH_2=N-CH_3)$ = 9.14 eV and the vertical ionization energy $IE_v(CH_2=N-CH_3)$ = 9.96 eV at the G3 level of theory. This reinforces the

assignment of the neutral species to CH_2=$\dot{N}CH_3$, $^1A'$ (C_s), formed by secondary dissociation of $N(CH_3)_2$ radicals:

$$N(CH_3)_3 + 193\ nm \rightarrow N(CH_3)_2\ (\tilde{X}^2B_1) + CH_3 \qquad D_0 = 77.6\ kcal/mol$$

$$\rightarrow CH_2{=}NCH_3 + H \quad D_0 = 31.9\ kcal/mol$$

The calculated minimum energy required for the secondary production of CH_2=NCH_3 is thus 109.5 kcal/mol (see Table V), which corresponds to a maximum of 39 kcal/mol remaining for relative product translation. The less precisely determined experimental enthalpy changes are smaller for each reaction above, giving a maximum of 44 kcal/mol available for product translation. The translational energy distribution for this reaction, the slower one in Figure 5, extends to 46 kcal/mol. The upper limit of this $P(E_T)$ is difficult to determine, however, because it assumes secondary H-atom loss from $N(CH_3)_2$ to have no impact on the velocity of the CH_2NCH_3 products. Within this assumption, the calculated and observed maximum translational energies are in quite reasonable agreement.

IVB. Shape and energetics of the TOF spectra at m/e=42

The photofragment TOF spectrum at *m/e*=42 obtained by 11 eV photoionization (see Figure 3) is very similar to that obtained using 200 eV electron impact ionization,[1] where the bulk of the signal is fit well with the two $P(E_T)$'s shown in Figure 5. Because the translational energies of the fastest products extend close to the limit of available energy following N-CH_3 bond

fission (compare E_{avl}=70±3 kcal/mol from G3 calculations with the maximum translational energy in the faster $P(E_T)$ in Figure 5), the higher kinetic energy distribution is attributed to $N(CH_3)_2$ ($\tilde{X}^2B_1$) radicals formed with little internal energy, which arrive intact at the detector.[1] Recall that the slower $P(E_T)$ was attributed in the previous subsection to unstable $N(CH_3)_2^*$ primary products which undergo secondary H-atom loss, which now are seen to appear also at *m/e*=42.

The shape of the *m/e*=42 TOF spectrum changes markedly at lower photoionization energy (see Figure 7 obtained at 10 eV), where not only are the different ionization efficiencies of the contributing species obvious, but the rising edge of the spectrum is also overfit by the faster $P(E_T)$. The change in the rising edge is puzzling, as this indicates ionization of only a slow subset of the $N(CH_3)_2$ reaction products. It is possible that the ionization is dependent on the internal energy of the radicals, and that at 10 eV, the fastest $N(CH_3)_2$ ($\tilde{X}^2B_1$) products (i.e., those with the least internal energy) are not being ionized. The ionization efficiency of polyatomic radicals is not usually so strongly dependent on internal energy, however, and if this explanation is true, it would represent a rather unusual case.

Also apparent in Figure 3 is additional slow TOF signal not fit by either of the $P(E_T)$'s shown in Figure 5. Similarly underfit slow signal at *m/e*=42 was observed in the experiments utilizing 200 eV EI ionization.[1] (The scatter in the

data points at lower ionization energies in e.g. Figure 7 may obscure the need for an additional slow distribution to fit this signal as well.) One possibility for the slow signal at *m/e*=42 is dissociative ionization of CH_2NCH_3 to *m/e*=42. We can discount this possibility by considering the shape of the TOF spectra following photoionization and 200 eV EI ionization: under 200 eV electron bombardment, ionization is relatively insensitive to the internal rovibrational state of the neutral species. Thus, if the slow species appearing at *m/e*=42 arose from dissociative ionization of CH_2NCH_3, an identical shape of the TOF distribution from this species should be observed at *m/e*=43 and *m/e*=42 following 200 eV EI ionization (after correcting for the ion flight time through the detector). This was not the case: the slow edge of the *m/e*=42 photofragment TOF spectrum was not observed at *m/e*=43.[1] Translational energy distributions for reactions (1) and (2), giving primary $N(CH_3)_2$ and secondary CH_2NCH_3 neutral reaction products, are used in fitting the data at *m/e*=42, and the remaining slow signal cannot be attributed to dissociative ionization of either species. As there are no other obvious neutral products of mass 44 or 43, we consider secondary dissociation of $N(CH_3)_2 \rightarrow NC_2H_4 + H_2$ as a possibility.

There is scant information available in the literature about nitrogen-containing radicals of formula NC_2H_4. Based on our experimental results, we can provide some energetic information for this slowest species of parent mass 42. If we assume that H_2 loss from $N(CH_3)_2$ occurs with little energetic barrier

(not likely to be a good assumption), the velocity distribution of recoiling NC_2H_4 should be similar to that of $N(CH_3)_2$. We can then determine a $P(E_T)$ for this signal, based on the times of flight of the momentum-matched CH_3 partners. Figure 4 shows a TOF spectrum recorded at *m/e*=15, at a 50• source angle, and with 10.5 eV probe photons. It is fit with the $P(E_T)$'s for reactions (1) and (2) shown in Figure 5, corresponding to CH_3 radicals momentum-matched to stable $N(CH_3)_2$ radicals and unstable $N(CH_3)_2^*$ radicals (that undergo secondary dissociation to CH_2NCH_3), respectively. There is no slow edge of this signal that is unfit, i.e., we cannot find CH_3 radicals momentum-matched to the slower NC_2H_4 radicals appearing at *m/e*=42. This is not overly surprising, as it is likely that H_2 loss provides a velocity "kick" to the recoiling NC_2H_4 radicals, such that their times of arrival at the detector are broadened to fast and particularly to slow times compared to the methyl radicals that are momentum-matched to the unstable $N(CH_3)_2^\dagger$ precursor. The best we can do then is to fit the slow portion of the *m/e*=42 TOF distribution to a velocity distribution, P(v), of the neutral precursor to the signal at *m/e*=42. Doing this fits the slow portion of the TOF spectrum (see Figure 8) with the P(v) shown in Figure 9. If this distribution corresponds to primary dissociation to unstable $N(CH_3)_2^\dagger + CH_3$, we can obtain a $P(E_T)$ by converting from velocity to recoil translational energy. The $P(E_T)$ thus derived extends from 0-24 kcal/mol. This $P(E_T)$ is likely broader than the "true"

primary $P(E_T)$, due to the probable exit barrier to H_2 loss and concomitant velocity kick imparted to the NC_2H_4 radicals.

The upper limit of the $P(E_T)$, assuming primary dissociation to unstable $N(CH_3)_2^{\dagger}$ + CH_3, can be used to find the minimum internal energy of the $N(CH_3)_2^{\dagger}$ radicals that go on to lose H_2 and form NC_2H_4 radicals. The primary dissociation, $N(CH_3)_3 \rightarrow N(CH_3)_2 + CH_3$ has been calculated at the G3 level to have D_0= 77.6 kcal/mol, with an estimated error of ±2-3 kcal/mol. The available energy following 193 nm excitation and N-CH_3 bond fission is then given by (148 - 78=) 70 kcal/mol. The upper limit of the $P(E_T)$ derived from the P(v) shown in Figure 9 is 24 kcal/mol, corresponding to an internal energy of $N(CH_3)_2$ radicals of (70 - 24=) 46 kcal/mol, assuming formation of internally cold CH_3 radicals. This value provides a very rough estimate of the energy required to undergo secondary H_2 loss from $N(CH_3)_2$.

Possible radical structures with chemical formula NC_2H_4 and the related enthalpies of reaction (at the G3 level of theory) are as follows:

$N(CH_3)_2$	$\rightarrow$	$CH_2NCH_2 + H_2$	ΔH = 15.7 kcal/mol
		$CHNCH_3 + H_2$	ΔH = 24.8 kcal/mol
		$H_2C\underline{N}CH_2$ (ring) + H_2	ΔH = 33.4 kcal/mol

All of these possible structures are energetically accessible, and we now turn to the ion appearance energies at *m/e*=42 for additional information that may help in identifying this species.

IVC. Ionization characteristics of the species appearing at m/e=42: $N(CH_3)_2$, CH_2NCH_3 *and* NC_2H_4

The photoion yield curve corresponding to *m/e*=42 can help identify the neutral species responsible for the signal. To that end, we have recorded TOF spectra at *m/e*=42 and a 30• source angle, varying the ionization energy from 8.7-10.7 eV. These TOF spectra were fit with the $P(E_T)$'s shown in Figure 5, with the addition of the slow P(v) shown in Figure 9. The "fast" distribution (the faster $P(E_T)$ in Figure 5) gave signal arriving from 90-118 μsec; the "middle" distribution (the slower $P(E_T)$ in Figure 5) gave signal arriving from 96-300 μsec; and the "slowest" distribution (the P(v) in Figure 9) gave signal arriving from 112-300 μsec. We first integrated the total signal arriving from 90-300 μsec, using the very minimal signal from 10-80 μsec for "background" subtraction and corrected the integrated signal intensity for variations in the probe power. This plot of the total photoionization yield at *m/e*=42 is shown in Figure 10. The curve hints at three contributions which may correspond to the three distributions used to fit the *m/e*=42 TOF spectra. The ion signal starts to appear around 9.0 – 9.1 eV, and, after a modest increase, quickly levels off. A second, slightly more pronounced contribution starts at ~9.5 eV, causing the ion yield to ascend nearly linearly until ~10.1 eV. At that point there appears to be a break in the slope, and a new, quasi-linear increase in the ion yield ensues, continuing to the highest energy point recorded here.

We have attempted to determine independently the partial photoion yield of each contribution, by integrating separately the signal over times of flight where each of the three $P(E_T)$'s (or P(v)) is dominant. Unfortunately, as seen in Figure 8, the arrival times of the three components overlap to a great extent, making a clean separation of the three components difficult to achieve. Consequently, the resulting partial spectra are "cross-contaminated". In addition, the three partial photoionization yield curves have significantly larger scatter than the total photoion yield curve, making the interpretation even more difficult.

Figure 11 shows the partial photoion efficiency curve for the fastest signal at *m/e*=42, obtained by integrating the time of flight between 90-100 μsec. At the earliest of these flight times, only the fast channel contributes, and over the rest of this integration range, the relative intensity of the middle distribution is less than 10% of that of the fast distribution. The partial photoion yield in Figure 11 has an apparent onset at ~9.1 eV, after which the curve ascends in a gently rounded fashion until ~10.2 eV, where it shows a tendency to level off. This is followed by a further increase given by a few scattered points at higher energies, although it is not entirely clear whether this belongs to the "fast" component or represents a "contamination" from the middle component. A comparison with the total yield in Figure 10 suggests that the fastest component is predominantly responsible for the portion of the total yield at lowest energies.

The overall shape of the spectrum in Figure 11 is very suggestive of parent ionization. The adiabatic ionization onset is at ~9.1 eV (or lower) with the vertical ionization energy very roughly 0.6-0.7 eV higher. These values do not match the predicted ionization energies for either CH_2NCH_2 or CH_3NCH (see Table IV). However, they show excellent agreement with the predicted adiabatic and vertical ionization energies of CH_3NCH_3. The calculated adiabatic ionization energy of CH_3NCH_3 to the triplet cation of similar structure (dimethyl nitrenium) is predicted to be 9.0 eV, and to the singlet cation to be 9.1 eV, both coinciding with the discernible onset in Figure 11. Furthermore, the predicted vertical ionization energies of dimethyl amidogen to the singlet and triplet ionic surfaces are 9.7 and 9.8 eV, respectively, quite close to the middle of the initial rise in Figure 11.

Why is this signal seen at *m/e*=42, rather than at *m/e*=44, as would be expected normally from parent ionization of CH_3NCH_3? One obvious possibility is that the dimethyl nitrenium ion, $CH_3NCH_3^+$, initially formed by photoionization, is unstable and fragments promptly to $NC_2H_4^+ + H_2$. This suggestion is reinforced by the observation that at all explored energies in these experiments, we were unable to observe *m/e*=44 beyond the limit of $<10^{-3}$ of the intensity at *m/e*=43. Hence, the parent ion of CH_3NCH_3 gives, at best, extremely weak signal. Although the ionic species that is detected corresponds to a fragment, the onset and the shape of the photoionization efficiency curve are still

defined by the Franck-Condon factors corresponding to the initial transition from the CH_3NCH_3 neutral to the $CH_3NCH_3^+$ surface(s). This is because a direct transition from the CH_3NCH_3 neutral to the $NC_2H_4^+ + H_2$ asymptote, although requiring less energy, does not contribute to the observable photoionization efficiency, since it would involve vanishingly small Franck-Condon factors.

While G3 calculations do find a minimum corresponding to $CH_3NCH_3^+$ on both the singlet and triplet surfaces, they also show that the fragmentation of $CH_3NCH_3^+$ to $NC_2H_4^+ + H_2$ has several exothermic paths, depending on the assumed structure of the $NC_2H_4^+$ ion. For example, the most stable ion of the $NC_2H_4^+$ composition examined here, corresponding to N-protonated acetonitrile, CH_3-C≡N^+-H, $^1A_1$ (C_{3v}), corresponds to a fragmentation asymptote that is 51.7 kcal/mol downhill from the $CH_3NCH_3^+$ singlet ion. The rearrangement required to access this asymptote is generally facile on ionic surfaces (usually much more so than on neutral surfaces). A more exhaustive theoretical examination of the $NC_2H_4^+$ potential energy surfaces (at the MP2/6-31G(d)//4-31G level)[39] also found this ion to be the most stable structure on the singlet surface. The same study indicated that the lowest $NC_2H_4^+$ ion on the triplet surface is ~69 kcal/mol higher in energy, and hence does not provide an exothermic path for photodissociative ionization of dimethylamidogen on the triplet surface. It is not clear whether this by itself means that the triplet $CH_3NCH_3^+$ ion is more stable

than the singlet ion, since triplet-singlet intersystem crossings may lead to very efficient fragmentation of triplet ions via singlet dissociative states.[46-48]

Although we have not tried to estimate the depth of the $CH_3NCH_3^+$ minima, nor we have tried to identify the transition state that would lead to a $NC_2H_4^+ + H_2$ asymptote, prior theoretical studies do indicate that the dimethylnitrenium ion is not particularly stable. For example, Ford and Herman[37] found that at the MP2(full)/6-31G(d) level the $CH_3NCH_3^+$ ion does not correspond to a local minimum on the singlet surface, but to a transition state for H migration to the immonium ion ($CH_2NHCH_3^+$), while on the triplet surface the nitrenium ($CH_3NCH_3^+$) and immonium ions were found to lie within 0.2 kcal/mol. For comparison, at the G3 level of theory the immonium ion is also more stable than the nitrenium ion by 76.9 kcal/mol on the singlet surface, while on the triplet surface the immonium ion is less stable by 1.2 kcal/mol (see Table III).

Figure 12 displays the partial photoionization efficiency curve associated with the "middle" species at *m/e*=42, obtained by integrating the photofragment TOF spectra between 112 and 121 μsec. While it is very difficult to avoid contributions from both the "fast" and the "slow" components, the integration limits chosen here are an attempt to minimize these unwanted contributions by keeping their sum to less than 10% of the desired "middle" component. The partial spectrum of the "middle" component seems to correspond to the rise seen

at the high-energy end of the total photoionization efficiency spectrum presented in Figure 10.

The general shape of the spectrum in Figure 12 is strongly suggestive of a fragment resulting from photodissociative ionization of a heavier parent:[49,50] at higher energy there appears to be a quasi-linear ascent, which is preceded by a very prominent and rounded tail. Though the data is somewhat scattered and is complicated by the imperfect separation of the three component species, the quasi-linear ascent suggests that the appearance energy for the fragment in question is in the neighborhood of 9.8-9.9 eV. Technically, this value should be corrected for the average internal energy of the neutral parent, which may be available to the photodissociative ionization process. In the present case such correction is rather difficult to do reliably, and may not be particularly important, given the approximate nature of the extracted appearance energy and the expectation that the excess energy of the parent will not be particularly well randomized between the available internal modes.

Hence, the partial photoionization efficiency spectrum in Figure 12 suggests that the responsible neutral species has a m/e>42, with an adiabatic ionization energy substantially smaller than 9.8 eV, and which can produce a $NC_2H_4^+$ fragment ion with an appearance energy of 9.8 eV or larger. The candidate that best appears to fit these requirements is CH_2=N-CH_3, which is predicted to dissociatively ionize to the most stable isomer of $NC_2H_4^+$, N-

protonated acetonitrile ($H_3C\text{-}C{\equiv}N^+\text{-}H$) at 9.9 eV (see Table IV). Hence, the partial photoionization yield in Figure 12 is consistent with the assignment of the "middle" species (which also gives ionic signal at *m/e*=43) to $CH_2{=}NCH_3$, formed by secondary dissociation of the primary $N(CH_3)_2$ product.

Finally, we focus our attention to the remaining "slow" species. Unfortunately, as seen in Figure 8, over its entire range of TOF arrival times, signal from the "slow" species is overlapped by signal from the "middle" species. In order to minimize the contributions from the "middle" species, the TOF signal was integrated from 155-198 μsec, which corresponds to the range of arrival times at which the "slow" species contributes to 50±5 % of the total signal. The result is shown in Figure 13. Taking into account that the spectrum really corresponds to a superposition of two species, its shape suggests that the "slow" species is probably responsible for the feature in the center of the total photoion efficiency curve presented in Figure 10. To further reduce contamination by the "middle" species, one can subtract its contribution from the photoion yield spectrum shown in Figure 13. By scaling the "middle" photoion yield curve (Figure 12) by the ratio of intensities under the middle-fit TOF curve used to obtain Figures 12 and 13 (area under 155-198 μs : area under 112-121 μs), the contribution of the middle species can be reduced, giving a clearer indication of the photoion yield spectrum of the slowest species at *m/e*=42. The result is shown in Figure 14.

The scatter in the data in Figure 14 and the composite nature of the spectrum in Figure 13 permit only a tentative assignment of the source of the slow TOF signal. While far from unambiguous, the overall shape of these spectra suggests that the underlying photoionization process could be parent ionization of a species with a rather broad Franck-Condon envelope. The apparent onset is ~9.5-9.6 eV, while the presumed vertical ionization is quite difficult to extract, although is not likely to be lower than ~10.0 eV. Given the scatter in the data, a much lower (but weaker) ionization onset cannot be excluded.

If the interpretation of the spectrum in Figure 14 as parent ionization at *m/e*=42 is correct, than there are two neutral species that appear as plausible candidates, based on the assumption that they originate via secondary dissociation of the primary $N(CH_3)_2$ photodissociation product: CH_3NCH and CH_2NCH_2. The two species differ in the source of the H_2 elimination (α,α or α,γ), with the underlying assumption in both mechanisms being that the transition state for elimination does not cause a skeletal rearrangement.

Turning now to the calculations for help (Table IV), the adiabatic and vertical ionization energies of CH_3NCH to the singlet surface of the ion (6.2 and 7.7 eV, respectively) are much lower, while those to the triplet surface (10.9 and 12.0 eV) are much higher, than needed to explain the spectrum in Figure 14. For ionization of CH_2NCH_2 to the singlet surface, the calculated values also cannot be rationalized with the partial photoion yield spectrum, as the adiabatic and

vertical ionization energies to the singlet surface (6.8 and 8.6 eV) are too low to explain the apparent features. However, the adiabatic and vertical ionization energies of CH_2NCH_2 to the triplet surface, 9.4 and 10.3 eV, seem relatively close to the spectral features in Figure 14. This, of course, may be purely accidental, since it is hard to explain why ionization of CH_2NCH_2 to the singlet surface of the ion would be missing in Figure 14, unless (as witnessed by the large difference of 1.8 eV between the adiabatic and vertical ionization energy) this results in a very extended Franck-Condon envelope that corresponds to a weak feature not easily discernible above the background scatter.

A radical structure in which CH_2NCH_2 forms a ring is also a possibility. The apparent onset of ionization in Figure 13 is lower than adiabatic ionization either to the $^3B_1$ ion (9.9 eV) or to the $^1A_1$ ion (10.2 eV), but this may be a result of the low energy tail of the "middle" species, which is also present in that spectrum. Also in Figure 14, the apparent onset of ionization is lower than these calculated energies, but the small number of counts involved does not allow for a very quantitative interpretation of the spectrum. The vertical ionization energies to these surfaces (10.7 and 10.4 eV, respectively) show good agreement with the midpoint of the rise in photoion signal in Figures 13 and 14. Hence, the assignment of the "slow" species as the CH_2NCH_2 ring structure cannot be excluded.

A more thorough analysis, that would consider both other NC_2H_4 species formed by H_2 elimination from $N(CH_3)_2$ via skeletal rearrangement, as well as possible higher-energy isomers of NC_2H_6 or NC_2H_5 that produce $NC_2H_4^+$ fragment ions by photodissociative ionization (but with unstable parent ions), would perhaps shed more light on the nature of the "slow" species. In the absence of such analysis we cannot assign the "slow" species.

V. Discussion and Summary

Under soft photoionization conditions at the Advanced Light Source, we have been able to identify several products of trimethylamine photodissociation at 193 nm. We have identified at least two nitrogen-containing species, $N(CH_3)_2$ and CH_2NCH_3, and perhaps a third species corresponding to NC_2H_4.

The radical $N(CH_3)_2$ has an experimentally-determined ionization onset of 9.1±0.2 eV, which is interpreted as being close to its adiabatic ionization energy. The calculated adiabatic ionization energy at the G3 level is 9.0±0.1 eV, similar to previous results at the G1 and G2 level (9.1±0.1 eV) by Wright and Miller.[23] The experimental evidence presented here suggests that the $N(CH_3)_2^+$ ion formed by photoionization of neutral $N(CH_3)_2$ is unstable and very efficiently fragments on the timescale of the experiment to produce an ion of *m/e*=42.

Superficially, the ionization energy of CH_3-N-CH_3 found here appears similar to the value reported earlier by Fisher and Henderson (I.P. ≤ 9.42±0.1 eV),[8] determined in an electron-impact study of the $N(CH_3)_2$ radical

formed by pyrolysis of $(CH_3)_2NNH_2$ and $(CH_3)_2NNO$. Their reported value corresponds to the observed ionization onset at *m/e*=44. However, pyrolysis is known to be not a particularly clean method for producing radicals, since it tends to produce additionally a complex mixture of secondary species arising from equilibration to other isomers on the hot walls and recombination in the reaction vessel. For example, Fisher and Henderson also reported signals at *m/e*=45 and 43, interpreted as arising from ionization of dimethylamine, $NH(CH_3)_2$ and methylenemethylamine, $CH_3N{=}CH_2$. Hence, it is not clear *a priori* whether their signal at *m/e*=44 corresponds to direct ionization of CH_3-N-CH_3, as they suggested, or to some other isomer resulting from equilibration on the wall. In fact, it is not even clear whether their signal at *m/e*=44 arises from parent ionization or corresponds to dissociative ionization from a heavier species.

In a more recent photoelectron study, Chunhua *et al.* report an experimental ionization energy (9.01±0.02 eV) very close to the calculated ionization energy of $N(CH_3)_2$.[22] Their experiments, however, also examined the products of pyrolysis of $(CH_3)_2NNO$, and are thus subject to the drawbacks discussed in the previous paragraph. In this system, the photoelectron spectrum is rendered complex by prominent NO peaks, which mask the region of interest for $N(CH_3)_2$. Their determination of the ionization energy rests on the presence of a single peak, at 9.01 eV, which is followed by a four-member vibrational progression of 1980±60 cm^{-1} starting at 9.65 eV. The isolated peak is assigned as

formation of the ground state of $N(CH_3)_2^+$ ($^1A_1$ from their single-point DFT calculations), while the subsequent photoelectron system that displays a vibrational progression is assigned as the $^3B_1$ state of the ion. Their interpretation of the isolated peak corresponding to a system where only the 0-0 transition is present requires the singlet ground state of the ion to have a geometry very similar to neutral $N(CH_3)_2$. This is in contrast to our calculations, which show the geometries of neutral $N(CH_3)_2$ and its ions to be quite different: there is a large difference between adiabatic and vertical ionization energies for ionization to the singlet and to the triplet (0.6 eV and 0.8 eV, respectively). Additionally, our calculations find the $^3B_1$ state of the cation to be slightly more stable than the $^1A_1$ state (at both the G3 and B3LYP/6-311G(d,p) levels of theory), the reverse of their DFT result. Closer examination of their spectra suggests some inconsistencies with their interpretation. The total area under the isolated peak is much smaller than that under the system assigned to the triplet state of the ion (or any other photoelectron systems that follow at higher energy), making doubtful the assumption that they belong to same neutral species. However, if the $N(CH_3)^+$ ion is indeed unstable or only marginally stable, as it appears from the present study, then the corresponding photoelectron features are expected to be significantly broadened by the short lifetime of the ion. Also, the vibrational progression of 1980 cm^{-1}, observed in their second system, is difficult to rationalize with a $N(CH_3)_2$ species, since it falls within the gap straddled at the

high end by C-H stretches (~2900 cm^{-1} and up) and at the low end by CH_3 deformations (~1650 cm^{-1} and down). Since photoelectron spectroscopy lacks mass analysis, it is not clear that the photoelectron feature at 9.01 eV observed by Chunhua *et al.* correlates with the formation of an ion of *m/e*=44. Assuming that it does nevertheless belong to ionization of $N(CH_3)_2$, a tentative explanation could be that it corresponds to the v=0 ionic level, which happens to have a sufficiently long lifetime, while other photoelectron features are much broader and are hence too difficult to observe under their conditions.

Castleman and co-workers[21] reported a lower (9.2±0.2 eV) and upper (9.9±0.2 eV) limit to the appearance energy of the fragmentation process:

$$NH(CH_3)_2 \rightarrow NC_2H_6^+ + H$$

While the resulting ion has *m/e*=44, they suggested that its structure is $CH_2NHCH_3^+$ rather than $CH_3NCH_3^+$. Indeed, using $\Delta H^\circ_{f\,298}(NH(CH_3)_2)$ = -4.7±0.5 kcal/mol[5] (0.5±0.5 kcal/mol at 0 K) with the 9.2-9.9 eV range for the appearance energy, one obtains $\Delta H^\circ_{f,0}(NC_2H_6^+)$ in the range of 165±5 to 175±5 kcal/mol, very close to our calculated enthalpy of formation for the singlet ground state of $CH_2NHCH_3^+$ (see Table III). Other experiments (notably those of Levsen and McLafferty[51] and Thon *et al.*[52]) that sought an ion of structure $N(CH_3)_2^+$, observed no signal at *m/e*=44 following 70 eV ionization. Thon *et al.* studied the thermal decomposition of trimethylamine, and found the intensity of their suspected $N(CH_3)_2$ primary product at *m/e*=44 to be very low (below the error limit);

however, the signal they observed at *m/e*=42 was strong. (They made no mention of signal at *m/e*=43.) Levsen and McLafferty, who used collisional activation, characterized the decomposition of ions of formula $NC_2H_6^+$, produced from various sources including trimethylamine. They found no peak at *m/e*=44, and concluded that ions of initial structure $CH_3NCH_3^+$ rearrange to $CH_3NH{=}CH_2^+$ faster than the 10^{-5} second drift time in their experiments. Then, depending on the amount of internal excitation of the latter ion, H-atom or H_2-molecule loss occurs, giving rise to the observed signals at *m/e*=43 and *m/e*=42. In addition, they noticed that high internal energies favor H-loss, while low internal energies increase the H_2-loss channel. This seems to match our observation, where the fastest primary $N(CH_3)_2$ photoproducts (i.e., those with the least internal energy) appear only at *m/e*=42, following H_2 loss in the ion. Our calculations show that the fragmentation of $N(CH_3)_2^+$ to $NC_2H_4^+ + H_2$ can be exoergic by ~50 kcal/mol, if the $NC_2H_4^+$ ion corresponds to the N-protonated acetonitrile, helping to explain how H_2 loss can occur even from those $N(CH_3)_2$ radicals with very little internal energy. The lack of any parent signal at *m/e*=44 at near-threshold photoionization conditions implies that this fragmentation has a very low barrier.

The CH_2NCH_3 closed-shell species formed in these experiments by secondary H-atom loss from $N(CH_3)_2$ has an experimentally-determined ionization onset of <9.3 eV. The calculated adiabatic ionization energy is 9.1 eV,

while the vertical ionization energy from internally cold CH_2NCH_3 is predicted to lie near 10 eV. Comparison with literature values places the experimental and adiabatic values towards the low end of previous observations[5] (ranging from 9.3-10.0 eV; see Table I), while the calculated vertical value is in agreement with the higher values, which also correspond to vertical ionization energies. In our experiments, signal from CH_2NCH_3 appears not only at its parent ion *m/e*=43 but also as a fragment at *m/e*=42. The calculated appearance energy for CH_3-C-NH^+ fragment ions of $CH_3NCH_2^+$ is 9.9 eV, while the experimentally observed onset (uncorrected for the effect of the internal energy excitation) is ~9.8-9.9 eV. The close agreement between these values, together with the agreement of our ionization onset with previous observations and calculations, support our assignment of the "middle" distribution to CH_2NCH_3 closed-shell species, formed by secondary dissociation of $N(CH_3)_2$ primary photoproducts.

Additionally, we have attempted to characterize the slowest species appearing at *m/e*=42. It would appear that this slowest channel arises from an internally hot primary $N(CH_3)_2$ photofragment undergoing secondary H_2 loss. We were not able to study the H_2 molecule TOF distributions, and so this assignment is based solely on the inferred photoionization properties of the slowest signal at *m/e*=42. Comparison of the photoion yield spectra (which suggest an ionization onset of 9.5-9.6 eV) with calculated adiabatic and vertical ionization energies does not allow us to definitively assign this species. Studies

utilizing higher resolution photoionization will be of great assistance in better characterizing this species. Additionally, the paucity of information in the literature on nitrogen-containing radicals of formula NC_2H_4 leaves the results of the present study awaiting further experiments and calculations in order to definitively assign this species. The results of this work provide a starting point for future studies on the NC_2H_4 radical, while also providing new information on the dissociation dynamics of the primary $N(CH_3)_2$ radical products of the photodissociation of trimethylamine at 193 nm. The dissociation dynamics of nitrogen-containing systems have proven to be rich and complex, containing surprisingly unstable $N(CH_3)_2$ radicals, and provide a fertile ground for further studies.

Acknowledgements

This work was supported by the Division of Chemical Sciences, Office of Basic Energy Sciences, Office of Energy Research, U.S. Department of Energy, under Grant No. DE-FG02-92ER14305 (N.R.F. and L.J.B.) and Contract No. W-31-109-ENG-38 (B.R.); and by the Director, Office of Science, Office of Basic Energy Sciences, Chemical Sciences Division of the U.S. Department of Energy under contract No. DE-AC03-76SF00098 (O.S., F.Q. and A.S.). The ALS is supported by the Director, Office of Science, Office of Basic Energy Sciences, Materials Sciences

Division of the U. S. Department of Energy under the latter contract. We acknowledge helpful discussions with M. L. Morton.

Table I – Literature values for the experimental enthalpies of formation and ionization energies of several species of interest in this paper.

Species	$\Delta H^\circ_{f,298}$ (kcal/mol)	Ionization Energy (eV)
$N(CH_3)_3$	-5.67 ± 0.18 [5,6]	7.76 - 8.56;[5] 7.85±0.05 (eval.)[5]
$CH_2N(CH_3)_2$	31.1 ± 2.4 [7,a]	
$N(CH_3)_2$	•30.3 [8] 33.7 [9] 33.8 ± 3 [10,b] 34 [11,12] 35 ± 2 [13] 39 [14] 29.3 ± 2 [15] 37.4 [16] 38.2 [17]	5.17[5] <9.42±0.1 [8] 9.01±0.02 eV [22,c]
CH_2NCH_3	11 ± 2 [5,18]	adiabatic: 9.3, 9.4, 9.8±0.1 [5] vertical: 10.0, 9.90±0.02 [5]
CH_2NCH_2	63 ± 3 [19]	

a. The value in reference 7 is for the bond dissociation energy of $N(CH_3)_3 \rightarrow CH_2N(CH_3)_2 + H$. We have used the values[5] of ΔH_f^0 for $N(CH_3)_3$ and H to determine an estimated ΔH_f^0 for $CH_2N(CH_3)_2$.

b. The published value for ΔH_f^0 of $N(CH_3)_2$ and bond enthalpies in Reference 10 are in error by 0.9 kcal/mol,[20] and so we have made the appropriate correction here.

c. A photoelectron value, not necessarily implying that the parent ion is stable.

Table II – Calculated enthalpies of formation of selected neutral species of interest to the present study. The values were obtained at the G3 level of theory and are listed at 0 K, with equivalent values at 298 K given in parentheses.

Species	**Calculated Enthalpy of Formation at 0 K (298 K), kcal/mol**	**Remark**
$N(CH_3)_3$, $^1A_1$ (C_{3v})	0.9 (-5.9)	
$CH_2N(CH_3)_2$, $^2A'$ (C_s)	40.4 (34.7)	
H_3C-N-CH_3, $^2B_1$ (C_{2v})	42.6 (38.6)	a
H_2C-NH-CH_3, ^2A (C_1)	40.2 (36.5)	
H_3C-N-CH_2, $^1A'$ (C_s)	22.9 (19.4)	b
H_3C-N-CH_2, $^3A''$ (C_s)	87.0 (83.8)	c
H_2C-NH-CH_2, $^1A'$ (C_s ring)	35.4 (31.4)	
H_2C-N-CH_2, $^2A_2$(C_{2v})	58.3 (55.7)	d
H_2C-N-CH_2, $^2B_1$(C_{2v} ring)	76.1 (73.1)	e
H_3C-N-CH, $^2A'$ (C_s, *1*)	67.4 (64.9)	f
H_3C-N-CH, $^2A'$ (C_s, 2)	72.0 (69.5)	g

a C_{2v} structure with a bent CNC frame, where on both sides one of the HCNC dihedral angles is 180•

b a C_s structure with a bent CNC frame, where on the CH_3 side one of the HCNC dihedral angles is 0•, while on the CH_2 side one of the HCNC dihedral angles is 0• and the other is 180•

c a C_s structure with a bent CNC frame, where on the CH_3 side one of the HNCN dihedral angles is 0•, while the CH_2 moiety is perpendicular to the CNC plane.

d planar C_{2v} structure with a bent CNC frame, where on both sides one of the HCNC dihedral angles is 0• and the other is 180•.

e ring C_{2v} structure

f a C_s structure with a bent CNC frame, where on the CH side the HCNC dihedral angle is 180•, while on the CH_3 side one of the HCNC dihedral angles is 0•

g a C_s structure with a bent CNC frame, where on the CH side the HCNC dihedral angle is 0•, and on the CH_3 side one of the HCNC dihedral angles is also 0•

Table III – Calculated enthalpies of formation of selected ionic species that are of interest to the present study. The values were obtained at the G3 level of theory and are listed at 0 K, with equivalent values at 298 K given in parentheses. The enthalpies of formation of ions follow the stationary electron convention (Ref. 53).

Species	**Calculated Enthalpy of Formation at 0 K (298 K), kcal/mol**	**Remark**
$N(CH_3)_3^+$, $^2A''$ (C_{3h})	182.3 (176.2)	
$H_3C\text{-}N\text{-}CH_3^+$, $^3B_1$ (C_{2v})	249.4 (245.7)	a
$H_3C\text{-}N\text{-}CH_3^+$, ^1A (C_2)	251.4 (247.2)	b
$H_2C\text{-}NH_2\text{-}CH_2^+$, $^1A_1$ (C_{2v} ring)	185.5 (180.6)	
$H_2C\text{-}NH\text{-}CH_3^+$, $^1A'$ (C_s)	174.5 (170.1)	c
$H_2C\text{-}NH\text{-}CH_3^+$, ^3A (C_1)	250.6 (246.8)	
$H_3C\text{-}N\text{-}CH_2^+$, $^2A'$ (C_s)	233.6 (230.6)	d
$H_2C\text{-}NH\text{-}CH_2^+$, $^2A'$ (C_s ring)	250.6 (246.8)	
$H_2C\text{-}N\text{-}CH_2^+$, $^1A_1(D_{2d})$	215.9 (213.3)	e
$H_2C\text{-}N\text{-}CH_2^+$, $^3A_2(C_{2v})$	276.1 (273.7)	f
$H_2C\text{-}N\text{-}CH_2^+$, $^1A_1(C_{2v}$ ring)	311.3 (308.6)	g
$H_2C\text{-}N\text{-}CH_2^+$, $^3B_1(C_{2v}$ ring)	303.3 (300.5)	g
$H_3C\text{-}N\text{-}CH^+$, $^1A_1$ (C_{3v})	211.0 (208.5)	h

$H_3C\text{-}N\text{-}CH^+$, $^3A''$ (C_s)	331.0 (328.7)	i
$H_3C\text{-}N\text{-}CH^+$, $^3A'$ (C_s)	318.8 (316.5)	j
$H_3C\text{-}C\text{-}NH^+$, $^1A_1$ (C_{3v})	199.6 (197.1)	k
$H_2C\text{-}C\text{-}NH_2^+$, $^1A_1$ (C_{2v})	215.3 (212.7)	l

a C_{2v} structure with a bent CNC frame, where on both sides one of the HCNC dihedral angles is 180•

b a C_2 structure where on each side one of the HCNC dihedral angles is ~7•; at the B3LYP level this corresponds to a C_{2v} structure where the two dihedral angles are 0•

c a C_s structure with a bent CNC frame, where the CH_2 and NH moieties and one of the H atoms on the CH_3 moiety (*trans* to the H atom on N) are in the CNC plane

d a C_s structure with a bent CNC frame, where on the CH_3 side one of the HCNC dihedral angles is 0•, while on the CH_2 side one of the HCNC dihedral angles is 0• and the other is 180•

e a D_{2d} structure with a linear CNC frame, where the two CH_2 moieties are perpendicular to each other

f planar C_{2v} structure with a bent CNC frame, where on both sides one of the HCNC dihedral angles is 0• and the other is 180•.

g ring C_{2v} structure

h a C_{3v} structure with a linear CNCH frame

i a C_s structure with a bent CNC frame, where on the CH side the HCNC dihedral angle is 180•, while on the CH_3 side one of the HCNC dihedral angles is 0•

j a C_s structure with a bent CNC frame, where on the CH side the HCNC dihedral angle is 0•, and on the CH_3 side one of the HCNC dihedral angles is also 0•

k a C_{3v} structure with a linear CCNH frame

l a C_{2v} structure with a linear CCN frame with the NH_2 and CH_2 moieties in perpendicular planes

Table IV – Calculated ionization energies and fragment appearance energies of interest to the present study. All values are at the G3 level of theory. IE_a and IE_v refer to the adiabatic and vertical ionization energies, respectively, while AE_0 [AB^+/ABC] is the 0 K appearance energy of the AB^+ ionic fragment formed by the photoionization process ABC + hν → AB^+ + C + e^-.

Quantity	**Calculated Value (eV)**
IE_a [$N(CH_3)_3$]	7.87
IE_a [H_3C-N-CH_3] to ^1A cation	9.05
IE_v [H_3C-N-CH_3] to singlet surface	9.68
IE_a [H_3C-N-CH_3] to $^3B_1$ cation	8.97
IE_v [H_3C-N-CH_3] to triplet surface	9.82
IE_a [H_3C-N-CH_3] to $^1A'$ ring cation	6.19
IE_a [H_3C-N-CH_3] to $^1A'$ (C_s) $CH_2NHCH_3^+$ cation	5.72
AE_0 [$CH_2NHCH_3^+$, $^1A'$ (C_s)/$N(CH_3)_3$]	9.08
AE_0 [$CH_2NHCH_3^+$, $^1A'$ (C_s)/$NH(CH_3)_2$]	9.73
IE_a [H_3C-N-CH_2] to $^2A'$ H_3C-N-CH_2^+ cation	9.14
IE_v [H_3C-N-CH_2]	9.96
IE_a [H_2C-NH-CH_2 ring] to $^2A'$ H_2C-NH-CH_2^+ ring cation	9.33
IE_v [H_3C-N-CH_2 ring]	10.00
AE_0 [CH_3-N-CH_2^+, $^2A'$ (C_s)/H_3C-N-CH_3, $^2B_1$ (C_{2v})]	10.52
AE_0 [H_2C-NH-CH_2^+, $^2A'$ (C_s ring)/H_3C-N-CH_3, $^2B_1$ (C_{2v})]	11.25

IE_a [H_2C-N-CH_2] to $^1A_1$ cation	6.83
IE_v [H_2C-N-CH_2] to singlet surface	8.63
IE_a [H_2C-N-CH_2] to $^3A_2$ cation	9.45
IE_v [H_2C-N-CH_2] to triplet surface	10.29
IE_a [H_2C-N-CH_2 $^2B_1$ ring] to $^1A_1$ ring	10.20
IE_v [H_2C-N-CH_2 $^2B_1$ ring] to singlet surface	10.42
IE_a [H_2C-N-CH_2 $^2B_1$ ring] to $^3B_1$ ring	9.85
IE_v [H_2C-N-CH_2 $^2B_1$ ring] to triplet surface	10.57
IE_a [H_3C-N-CH $^2A'$ (C_s, *1*)] to $^1A_1$ cation	6.23
IE_v [H_3C-N-CH $^2A'$ (C_s, *1*)] to singlet surface	7.70
IE_a [H_3C-N-CH $^2A'$ (C_s, *1*)] to $^3A'$ cation	10.90
IE_v [H_3C-N-CH $^2A'$ (C_s, *1*)] to triplet surface	11.98
IE_a [H_3C-N-CH $^2A'$ (C_s, *2*)] to $^1A_1$ cation	6.03
IE_v [H_3C-N-CH $^2A'$ (C_s, *2*)] to singlet surface	7.69
IE_a [H_3C-N-CH $^2A'$ (C_s, *2*)] to $^3A'$ cation	10.70
IE_v [H_3C-N-CH $^2A'$ (C_s, *2*)] to triplet surface	11.07
AE_0 [CH_2-N-CH_2^+, $^1A_1$ (D_{2d})/H_3C-N-CH_2, $^1A'$ (C_s)]	10.61
AE_0 [CH_3-N-CH^+, $^1A_1$ (C_{3v})/H_3C-N-CH_2, $^1A'$ (C_s)]	10.40
AE_0 [CH_3-C-NH^+, $^1A_1$ (C_{3v})/H_3C-N-CH_2, $^1A'$ (C_s)]	9.90

Table V – Calculated bond dissociation energies of interest to the present study. All values were calculated at the G3 level of theory at 0 K, with equivalent values at 298 K listed in parentheses.

Quantity	**Calculated Value at 0 K (298 K)**	**Remark**
$N(CH_3)_3 \rightarrow CH_2N(CH_3)_2 + H$	91.2 (92.7)	
$N(CH_3)_3 \rightarrow CH_3\text{-}N\text{-}CH_3 + CH_3$	77.6 (79.6)	a, b
$N(CH_3)_3 \rightarrow CH_2\text{-}NH\text{-}CH_3 + CH_3$	75.2 (77.4)	a, c
$CH_3\text{-}N\text{-}CH_3 \rightarrow CH_2\text{-}N\text{-}CH_3 + H$	31.9 (32.9)	
$CH_3\text{-}N\text{-}CH_3 \rightarrow CH_2\text{-}N\text{-}CH_2 + H_2$	15.7 (17.1)	
$CH_3\text{-}N\text{-}CH_3 \rightarrow CH_3\text{-}N\text{-}CH + H_2$	24.8 (26.3)	
$CH_3\text{-}N\text{-}CH_3 \rightarrow H_2C\underline{\underline{N}}CH_2 + H_2$	33.4 (34.5)	

a $\Delta H^\circ_{f0}(CH_3) = 35.86 \pm 0.07$ kcal/mol from Ref. 54.
b direct bond breakage to $^2B_1$ dimethyl amidogen
c requires rearrangement

Figure Captions

Figure 1 – Mass spectral sweep of photofragments at 10.5 eV over the range from *m/e*=42-44, showing that there are peaks at *m/e*=42 and *m/e*=43, but that the signal decreases monotonically past *m/e*=43 to *m/e*=44. There is no evidence for parent $N(CH_3)_2^+$ ion signal at *m/e*=44.

Figure 2 – TOF spectrum of the products of trimethylamine photodissociation at 193 nm, recorded at *m/e*=43, at a 30• source angle, and with 10.5 eV ionization energy. Experimental points are shown as open circles and the fit to the data is given as a solid line. The experimental data are fit beautifully by the same translational energy distribution ($P(E_T)$) that was used previously (Ref. 1) to fit the signal observed at *m/e*=43 following 200 eV electron-impact ionization of the photofragments of trimethylamine (see also Figure 5).

Figure 3 - TOF spectrum of the products of trimethylamine photodissociation at 193 nm, recorded at *m/e*=42, at a 30• source angle, and with 11 eV ionization energy. Experimental points are shown as open circles and the fit to the data is given as a solid line, with contributions from dissociation channels shown as broken lines. The fit uses the translational energy distributions ($P(E_T)$'s)

determined previously from electron impact data (Ref. 1, see also Figure 5), which leave the slow edge inadequately fit.

Figure 4 - TOF spectrum of the products of trimethylamine photodissociation at 193 nm, recorded at *m/e*=15, at a 50• source angle, and with 10.5 eV ionization energy. Experimental points are shown as open circles and the fit to the data is given as a solid line, with contributions from dissociation channels shown as broken lines. The fit uses the translational energy distributions ($P(E_T)$'s) determined previously from electron impact data (Ref. 1, see also Figure 5).

Figure 5 – Recoil translational energy distributions ($P(E_T)$'s) used to fit the TOF spectra both in this paper and in previous work (Ref. 1) that used 200 eV electron-impact ionization.[1] The faster $P(E_T)$, extending from 26-66 kcal/mol, was assigned previously (Reference 1) to $N(CH_3)_2$ ($\tilde{X}^2B_1$) + CH_3. The slower $P(E_T)$ shown here, extending from 0-46 kcal/mol, corresponds to primary formation of unstable $N(CH_3)_2$* + CH_3, where the $N(CH_3)_2$ radical undergoes secondary H-atom loss prior to its arrival at the detector.

Figure 6 –Photoion yield curve for the species appearing at *m/e*=43. The TOF signal at *m/e*=43 was integrated from 96-300 μsec, and the intensity shown in this

plot has been corrected for variations in the probe photon flux. We have attributed this signal to the ionization of neutral CH_2NCH_3 secondary products.

Figure 7 - TOF spectrum of the products of trimethylamine photodissociation at 193 nm, recorded at *m/e*=42, at a 30• source angle, and with 10 eV ionization energy. Experimental points are shown as open circles connected by thin lines, the fit to the data is given as a solid line, and contributions from dissociation channels are shown as broken lines. The fit uses the translational energy distributions ($P(E_T)$'s) determined previously from electron impact data (Ref. 1, see also Figure 5). At this ionization energy, the TOF spectrum is bimodal, and the fit to the data appears to be too broad, especially for the fast peak. Reasons for this effect are discussed in the text.

Figure 8 – The same experimental TOF spectrum as that shown in Figure 3, clearly demonstrating that the P(v) shown in Figure 9 fits the slow edge of the signal.

Figure 9 – A velocity distribution, P(v), that can be used to fit the slowest, previously unfit portion of the signal at *m/e*=42. (See also Figure 8.)

Figure 10 – Total photoionization efficiency curve for all species appearing at *m/e*=42. The TOF signal at *m/e*=42 was integrated from 90-300 μsec, and intensities have been corrected for variations in the probe photon flux. Three possible contributions can be seen in this plot, perhaps corresponding to the three distributions used to fit the *m/e*=42 TOF spectrum in Figure 8. The ion signal starts to appear around 9.0–9.1 eV, and levels off after a modest increase. A second contribution starts at ~9.5 eV, and the third contribution commences at ~10.0-10.1 eV.

Figure 11 – Partial photoionization efficiency curve corresponding to the fastest species appearing at *m/e*=42. The TOF signal at *m/e*=42 was integrated from 90-100 μsec, and the intensity shown in this plot has been corrected for variations in the probe photon flux. The spectrum can be attributed to neutral $N(CH_3)_2$ radicals, undergoing efficient dissociative ionization to $NC_2H_4^+$ fragment ions (see text).

Figure 12 – Partial photoionization efficiency curve corresponding to the middle species appearing at *m/e*=42. The TOF signal at *m/e*=42 was integrated from 112-121 μsec, and the intensity shown in this plot has been corrected for variations in the probe photon flux. The spectrum can be attributed to dissociative ionization of CH_2NCH_3 (see text).

Figure 13 - Partial photoionization efficiency curve corresponding to a superposition of the slowest and middle species appearing at *m/e*=42. The TOF signal at *m/e*=42 was integrated from 155-198 μsec, and the intensity shown in this plot has been corrected for variations in the probe photon flux.

Figure 14 - Partial photoionization efficiency curve corresponding to the slowest species appearing at *m/e*=42. This curve was obtained by subtracting from Figure 13 the photoion yield of the middle species at *m/e*=42 from 155-198 μsec (obtained by scaling Figure 12 by the ratio of area under the middle fit TOF curve from 112-121 μsec to the area from 155-198 μsec). This spectrum can be tentatively attributed to neutral NC_2H_4 radicals, formed from secondary dissociation of $N(CH_3)_2$ (see text).

References

1 N. R. Forde, M. L. Morton, S. L. Curry, S. J. Wrenn, and L. J. Butler, *J. Chem. Phys.* **111,** 4558 (1999).

2 N. R. Forde, T. L. Myers, and L. J. Butler, *Faraday Discuss.* **108,** 221 (1997).

3 N. R. Forde, L. J. Butler, and S. A. Abrash, *J. Chem. Phys.* **110,** 8954 (1999).

4 Y. T. Lee, J. D. McDonald, P. R. LeBreton, and D. R. Herschbach, *J. Phys. Chem.* **89,** 4744 (1969).

5 H. Y. Afeefy, J. F. Liebman, and S. E. Stein, in *NIST Standard Reference Database Number 69,* edited by W. G. W. G. Mallard and J. P. Linstrom (National Institute of Standards and Technology; http://webbook.nist.gov, Gaithersburg, MD, 1997).

6 J. D. Cox and G. Pilcher, *Thermochemistry of Organic and Organometallic Compounds* (Academic Press, New York, 1970).

7 D. D. M. Wayner, K. B. Clark, A. Rauk, D. Yu, and D. A. Armstrong, *J. Am. Chem. Soc.* **119,** 8925 (1997).

8 I. P. Fisher and E. Henderson, *Trans. Faraday Soc.* **63,** 1342 (1967).

9 Y. D. Orlov, E. A. Miroshnichenko, L. I. Korchatova, V. P. Vorobeva, and Y. A. Lebedev, *Zh. Fiz. Khim.* **70,** 1749 (1996).

10 D. F. McMillen and D. M. Golden, *Annu. Rev. Phys. Chem.* **33,** 493 (1982).

11 J. L. Franklin, J. G. Dillard, H. M. Rosenstock, J. T. Herron, K. Draxl, and F. H. Field, *Natl. Stand. Ref. Data Ser. Natl. Bur. Stand.* **26** (1969).

12 B. G. Gowenlock, P. P. Jones, and J. R. Majer, *Trans. Faraday Soc.* **57,** 23 (1961).

13 S. A. Lloyd, M. E. Umstead, and M. C. Lin, *J. Energ. Mater.* **3,** 187 (1985).

14 J. L. Franklin and D. K. Sen Sharma, *Adv. Mass Spectrom.* **6,** 947 (1974).

15 J. A. Kerr, *Chem. Rev.* **66,** 465 (1966).

16 S. W. Benson and H. E. O'Neal, , Vol. 21 (Nat. standards Ref. Data service, NBS (US), Washington, DC, 1970).

17 D. M. Golden, R. K. Solly, N. A. Gac, and S. W. Benson, *J. Amer. Chem. Soc.* **94,** 363 (1972).

18 R. A. L. Peerboom, S. Ingemann, N. M. M. Nico, and J. F. Liebman, *J. Chem. Soc. Perkin Trans.* **2,** 1825 (1990).

19 Y. G. Lazarou and P. Papaginnakoupulos, *J. Phys. Chem.* **97,** 4468 (1993).

20 D. M. Golden, *personal communication* (1999).

21 S. W. Sigsworth, R. G. Keesee, and A. W. Castleman, *J. Am. Chem. Soc.* **110,** 6682 (1988).

22 Q. Chunhua, H. Gongyi, and W. Dianxun, *J. Phys. Chem.* **103,** 1972 (1999).

23 T. G. Wright and T. A. Miller, *J. Phys. Chem.* **100,** 4408 (1996).

24 S. A. Abrash, D. M. Potts, and K. F. Freed, *in preparation* (2000).

25 X. Yang, J. Lin, Y. T. Lee, D. A. Blank, A. G. Suits, and A. M. Wodtke, *Rev. Sci. Instrum.* **68,** 3317 (1997).

26 P. A. Heimann, M. Koike, C. W. Hsu, M. Evans, C. Y. Ng, D. Blank, X. M. Yang, C. Flaim, A. G. Suits, and Y. T. Lee, *Proc. SPIE-Int. Soc. Opt. Eng.* **2856,** 90 (1996).

27 P. A. Heimann, M. Koike, C. W. Hsu, D. Blank, X. M. Yang, A. G. Suits, Y. T. Lee, M. Evans, C. Y. Ng, C. Flaim, and H. A. Padmore, *Rev. Sci. Instrum.* **68,** 1945 (1997).

28 A. G. Suits, P. Heimann, X. Yang, M. Evans, C.-W. Hsu, K.-t. Lu, Y. T. Lee, and A. H. Kung, *Rev. Sci. Instrum.* **66,** 4841 (1995).

29 D. P. Taylor, C. F. Dion, and E. R. Bernstein, *J. Chem. Phys.* **106,** 3512 (1997).

30 W. B. Tzeng, K. Narayanan, G. C. Chang, W. C. Tsai, and J. J. Ho, *J. Phys.*

Chem. **100,** 15340 (1996).

31 M. J. Frisch, G. W. Trucks, H. B. Schlegel, G. E. Scuseria, M. A. Robb, J. R. Cheeseman, V. G. Zakrzewski, J. A. Montgomery, R. E. Stratmann, J. C. Burant, S. Dapprich, J. M. Millam, A. D. Daniels, K. N. Kudin, M. C. Strain, O. Farkas, J. Tomasi, V. Barone, M. Cossi, R. Cammi, B. Mennucci, C. Pomelli, C. Adamo, S. Clifford, J. Ochterski, G. A. Petersson, P. Y. Ayala, Q. Cui, K. Morokuma, D. K. Malick, A. D. Rabuck, K. Raghavachari, J. B. Foresman, J. Cioslowski, J. V. Ortiz, B. B. Stefanov, G. Liu, A. Liashenko, P. Piskorz, I. Komaromi, R. Gomperts, R. L. Martin, D. J. Fox, T. Keith, M. A. Al-Laham, C. Y. Peng, A. Nanayakkara, C. Gonzalez, M. Challacombe, P. M. W. Gill, B. G. Johnson, W. Chen, M. W. Wong, J. L. Andres, M. Head-Gordon, E. S. Replogle, and J. A. Pople, GAUSSIAN 98 (Gaussian, Inc., Pittsburgh, PA, 1998).

32 S. Hammerum and T. I. Solling, *J. Amer. Chem. Soc.* **121,** 6002 (1999).

33 J. Henricksen and S. Hammerum, *Int. J. Mass Spectrom.* **179,** 301 (1998).

34 W. Koch and G. Frenking, *J. Phys. Chem.* **91,** 49 (1987).

35 M. B. Seasholtz, T. B. Thompson, and N. G. Nelson, *J. Phys. Chem.* **99,** 17838 (1995).

36 S. A. Shaffer, F. Turecek, and R. L. Cerny, *J. Amer. Chem. Soc.* **115,** 12117 (1993).

37 G. P. Ford and P. S. Herman, *J. Amer. Chem. Soc.* **111,** 3987 (1989).

38 V. Barone, F. Lelj, P. Grande, and N. Russo, *THEOCHEM* **25,** 319 (1985).

39 E.-U. Wurthwein, *J. Org. Chem.* **49,** 2971 (1984).

40 L. A. Curtiss, K. Raghavachari, P. C. Redfern, V. Rassolov, and J. A. Pople, *J. Chem. Phys.* **109,** 7764 (1998).

41 L. A. Curtiss, P. C. Redfern, K. Raghavachari, and J. A. Pople, *J. Chem. Phys.* **109,** 42 (1998).

42 L. A. Curtiss, K. Raghavachari, P. C. Redfern, and J. A. Pople, *J. Chem. Phys.* **106,** 1063 (1997).

43 A. D. Becke, *J. Chem. Phys.* **98,** 5648 (1993).

44 C. Lee, W. Yang, and R. G. Parr, *Phys. Rev. B* **37,** 785 (1988).

45 B. Miechlich, A. Savin, H. Stoll, and H. Preuss, *Chem. Phys. Lett.* **157,** 200 (1989).

46 B. Ruscic and J. Berkowitz, *J. Chem. Phys.* **95,** 4033 (1991).

47 B. Ruscic and J. Berkowitz, *Prepr. Pap. - Am. Chem. Soc., Div. Fuel Chem.* **36,** 1571 (1991).

48 D. Yarkony, *J. Amer. Chem. Soc.* **114,** 5406 (1992).

49 P. M. Guyon and J. Berkowitz, *J. Chem. Phys.* **54,** 1814 (1971).

50 W. A. Chupka, *J. Chem. Phys.* **54,** 1936 (1971).

51 K. Levsen and F. W. McLafferty, *J. Am. Chem. Soc.* **96,** 139 (1974).

52 A. Thon, D. Saulys, S. A. Safvi, D. F. Gaines, and T. F. Kuech, *J. Electrochem. Soc.* **144,** 1127 (1997).

53 H. M. Rosenstock, in *Kinetics of Ion-Molecule Reactions*, edited by P. Ausloos (Plenum, New York, 1979), pp. 246.

54 B. Ruscic, M. Litorja, and R. L. Asher, *J. Phys. Chem. A* **103,** 8625 (1999).

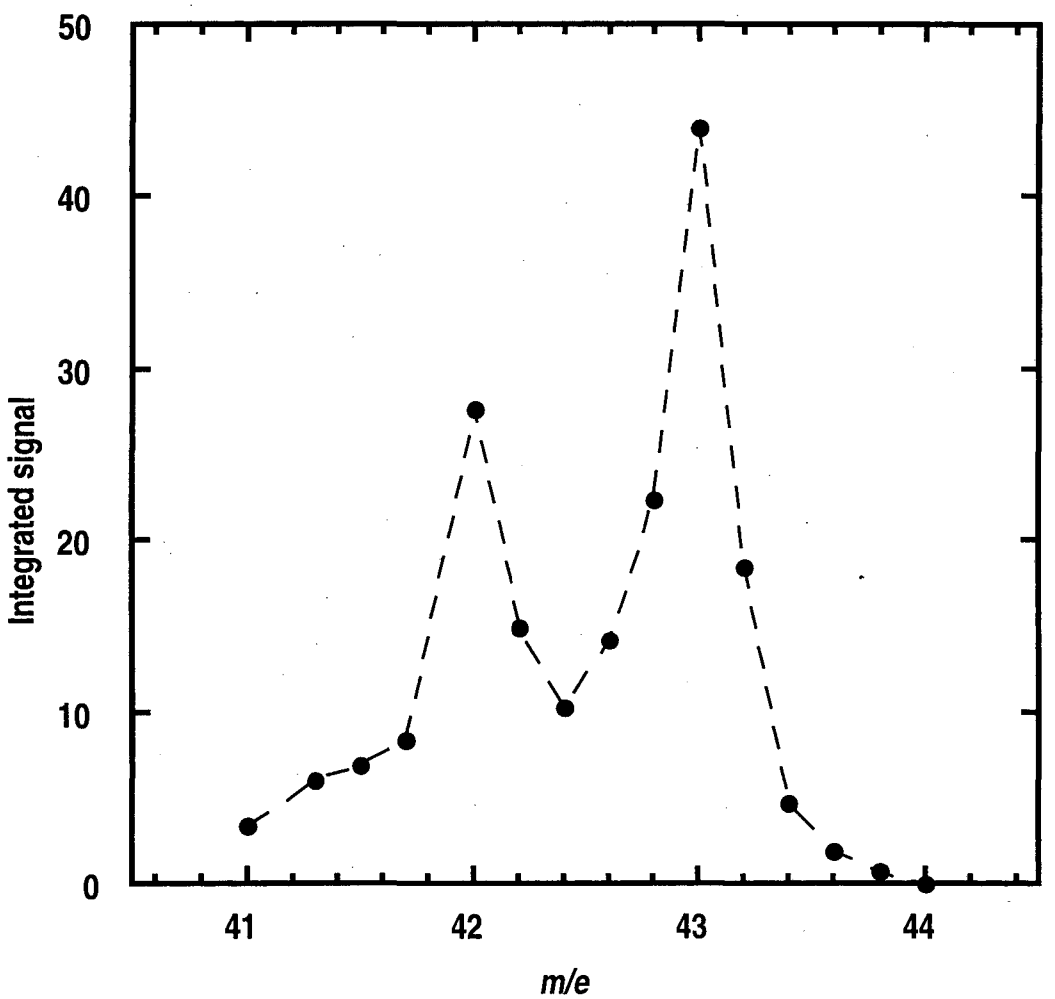

Fig 1

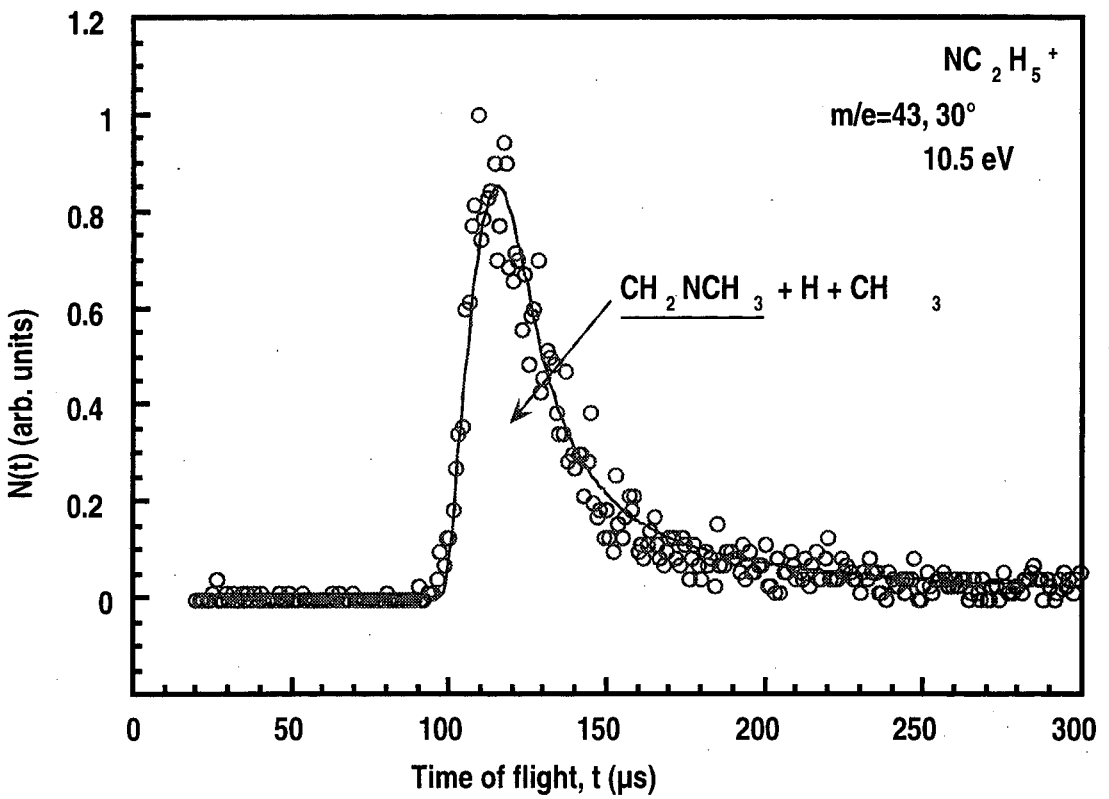
1.2
1
0.8
0.6
0.4
0.2
0
N(t) (arb. units)
NC 2 H 5 +
m/e=43, 30°
10.5 eV
CH 2 NCH 3 + H + CH 3
0
50
100
150
200
250
300
Time of flight, t (μs)

Fig 2

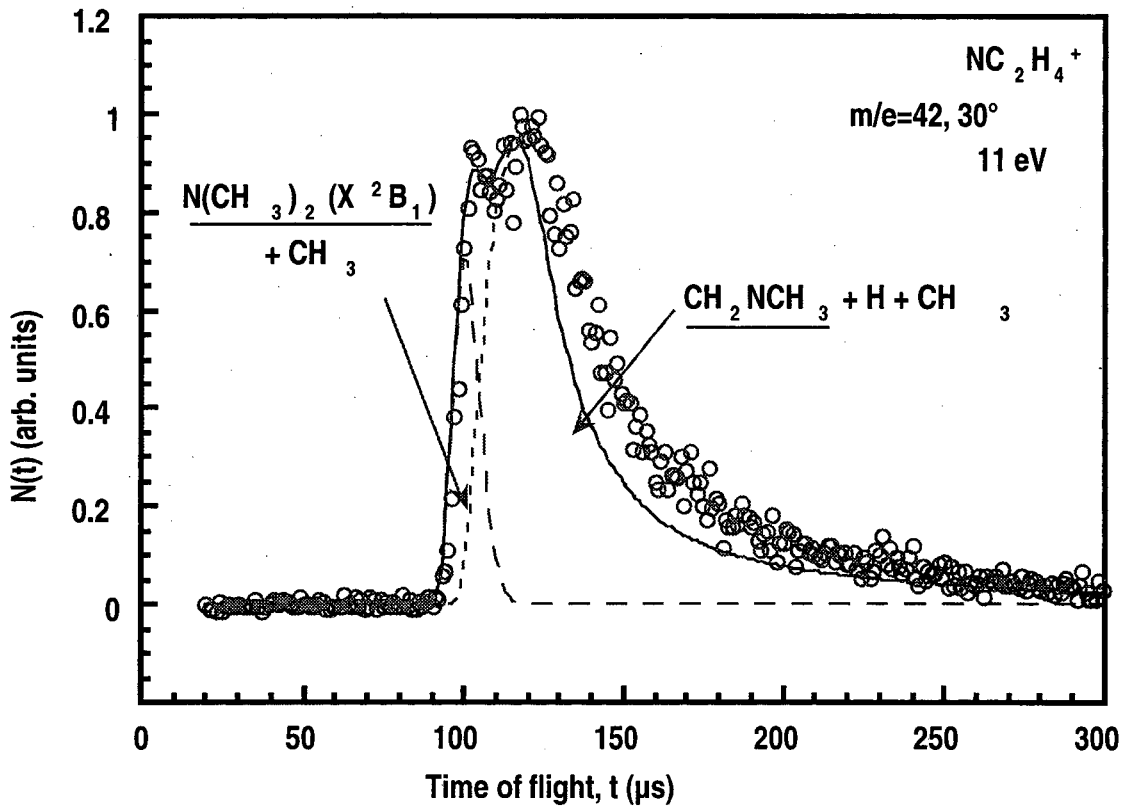
1.2
1
0.8
0.6
0.4
0.2
0
N(t) (arb. units)
0
50
100
150
200
250
300
Time of flight, t (μs)
NC 2 H 4 +
m/e=42, 30°
11 eV
N(CH 3) 2 (X 2B 1)
+ CH 3
CH 2 NCH 3 + H + CH 3

Fig 3

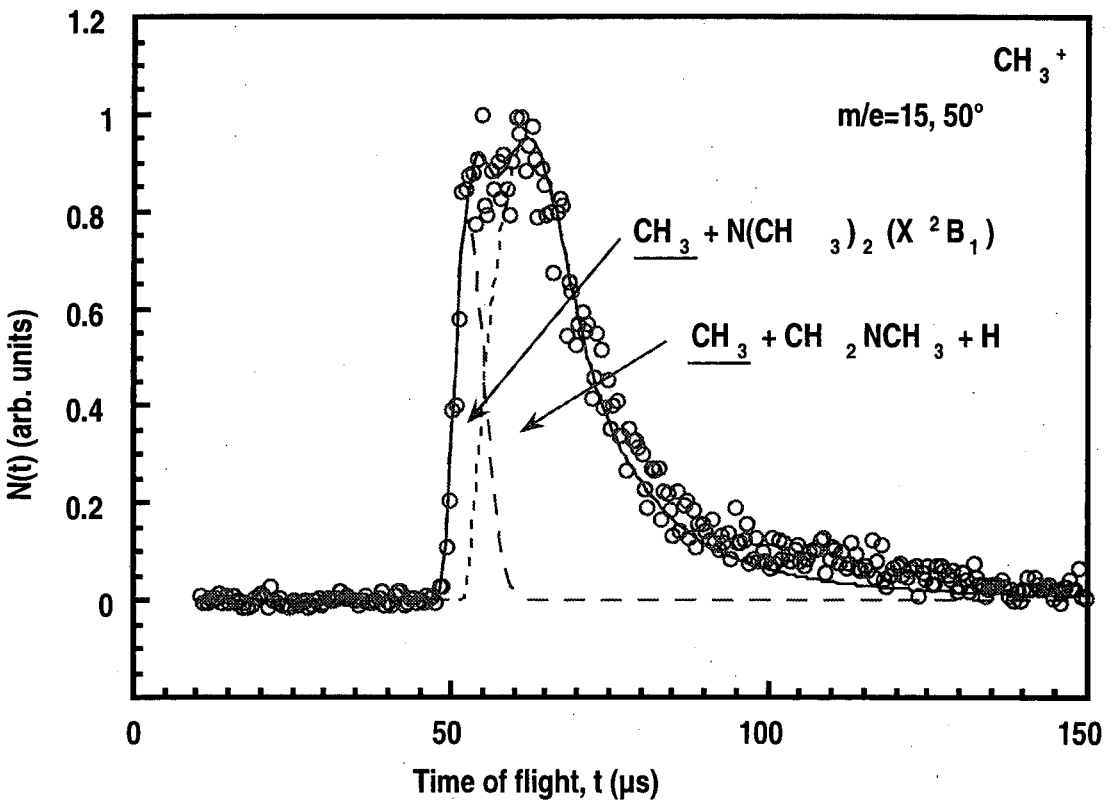
1.2
1
0.8
0.6
0.4
0.2
0
N(t) (arb. units)
0
50
100
150
Time of flight, t (μs)
CH3+
m/e=15, 50°
CH3 + N(CH3)2 (X 2B1)
CH3 + CH2NCH3 + H

Fig 4

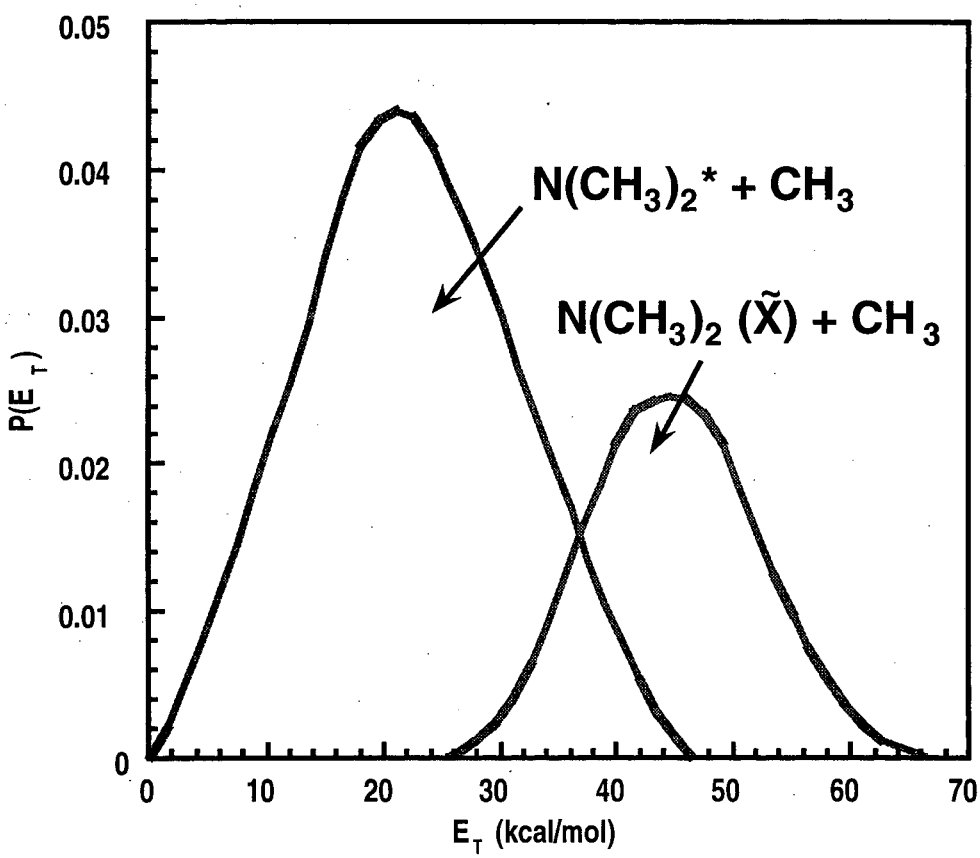
0.05
0.04
0.03
0.02
0.01
0
P(E T)
N(CH3)2* + CH3
N(CH3)2 (X̃) + CH3
0
10
20
30
40
50
60
70
ET (kcal/mol)

Fig 5

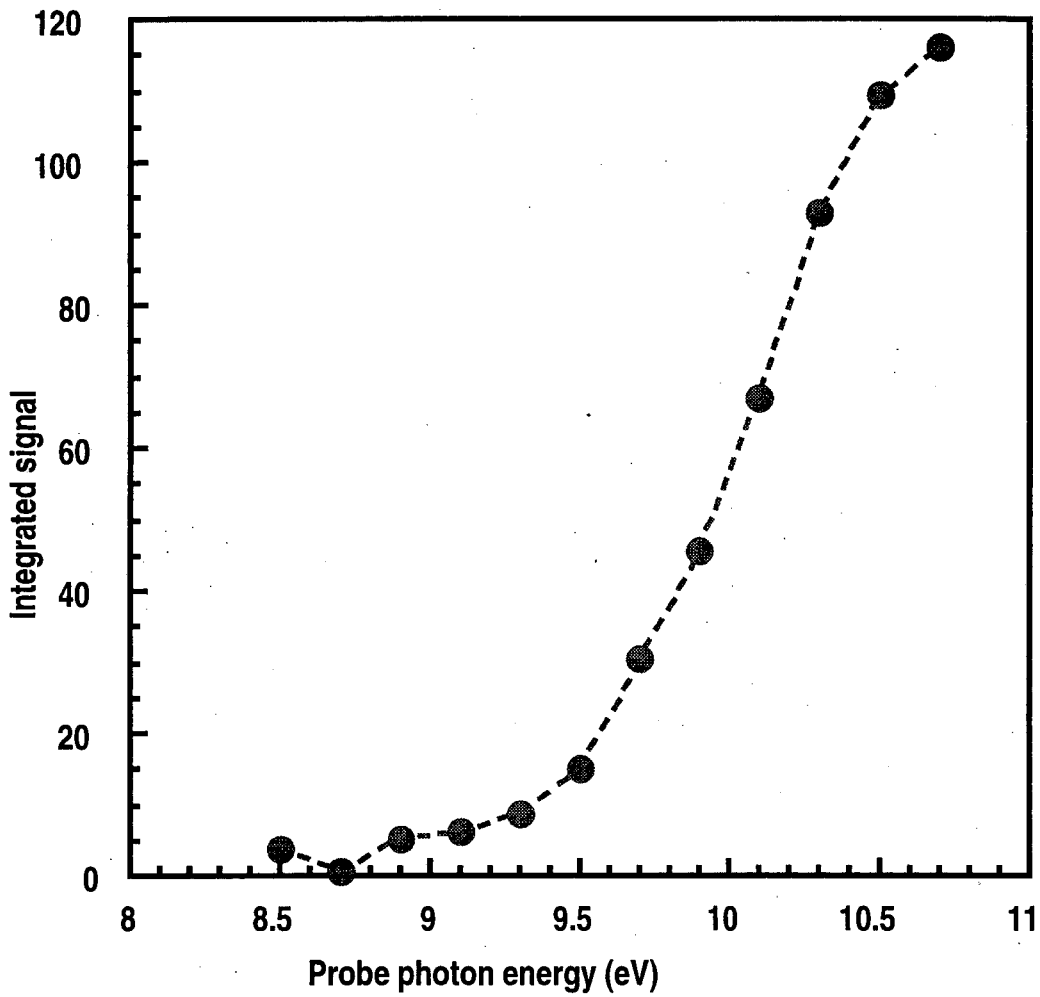
120
100
80
60
40
20
0
Integrated signal
8
8.5
9
9.5
10
10.5
11
Probe photon energy (eV)

Fig 6

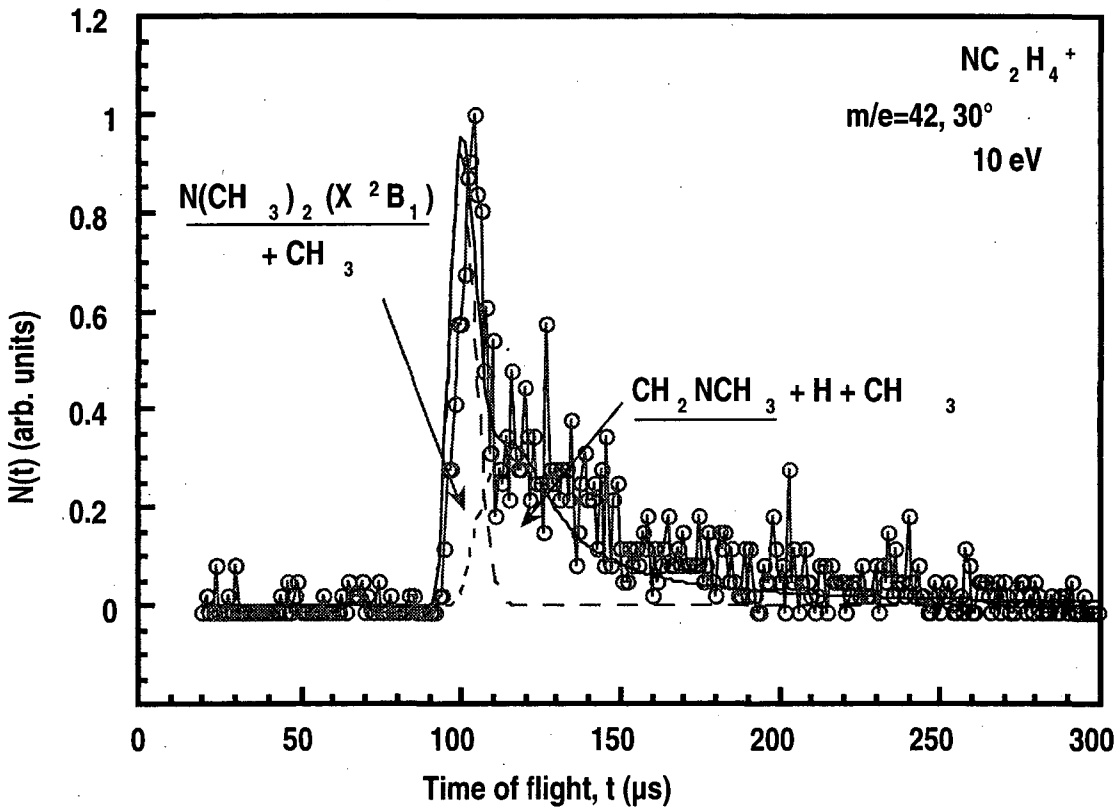
1.2
1
0.8
0.6
0.4
0.2
0
N(t) (arb. units)
0
50
100
150
200
250
300
Time of flight, t (μs)
NC 2 H 4 +
m/e=42, 30°
10 eV
N(CH 3) 2 (X 2 B 1)
+ CH 3
CH 2 NCH 3 + H + CH 3

Fig 7

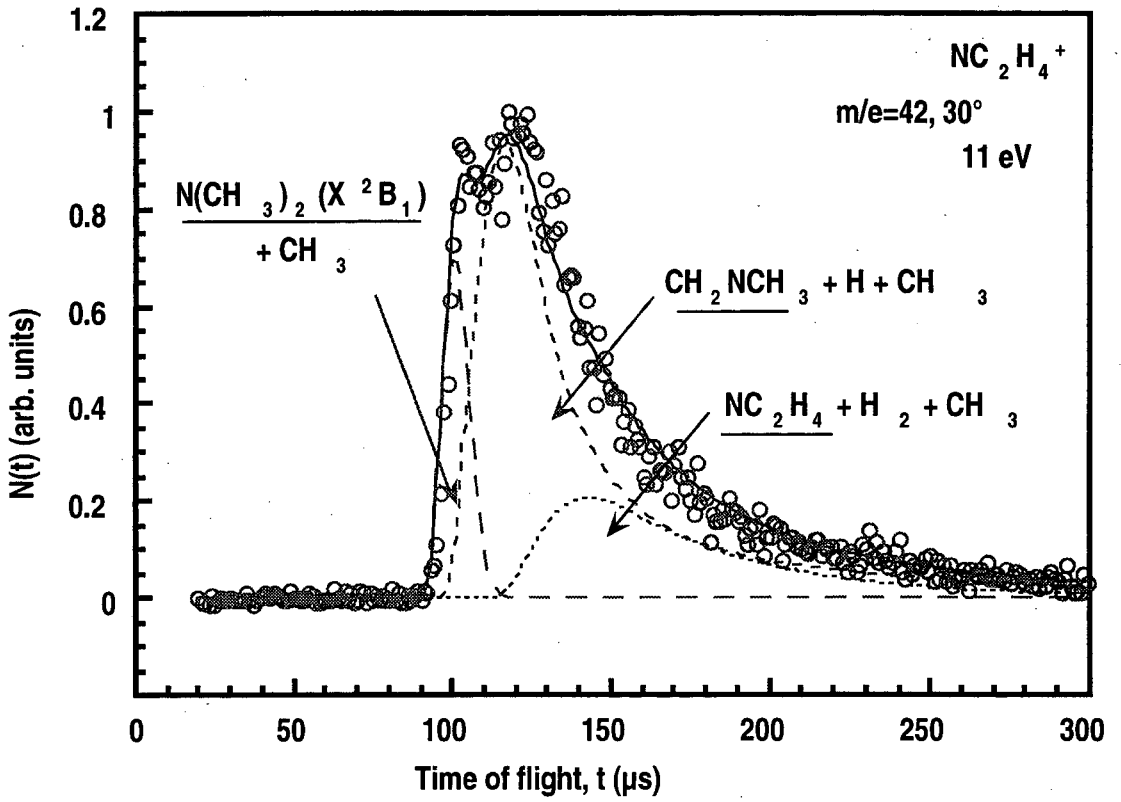
1.2
1
0.8
0.6
0.4
0.2
0
N(t) (arb. units)
0
50
100
150
200
250
300
Time of flight, t (μs)
NC 2 H 4 +
m/e=42, 30°
11 eV
N(CH 3) 2 (X 2 B 1)
+ CH 3
CH 2 NCH 3 + H + CH 3
NC 2 H 4 + H 2 + CH 3

Fig 8

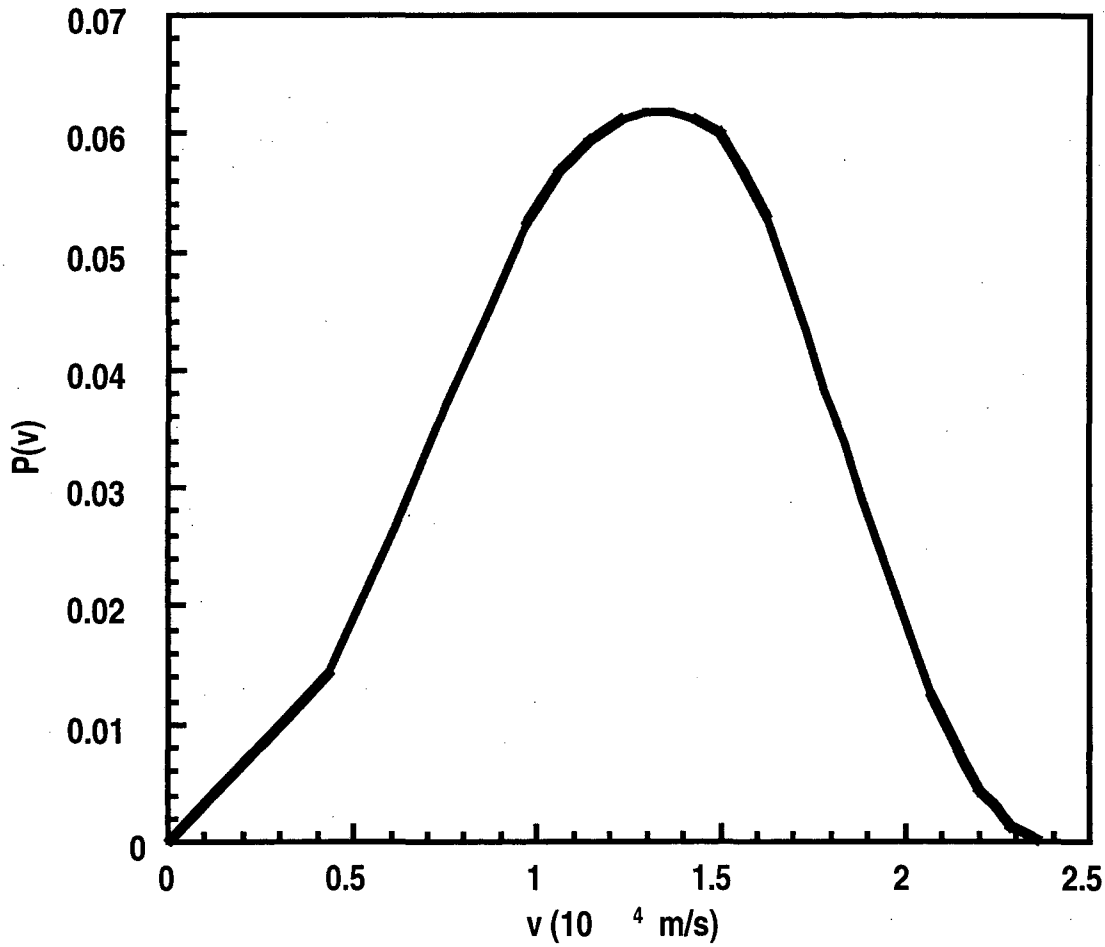

Fig 9

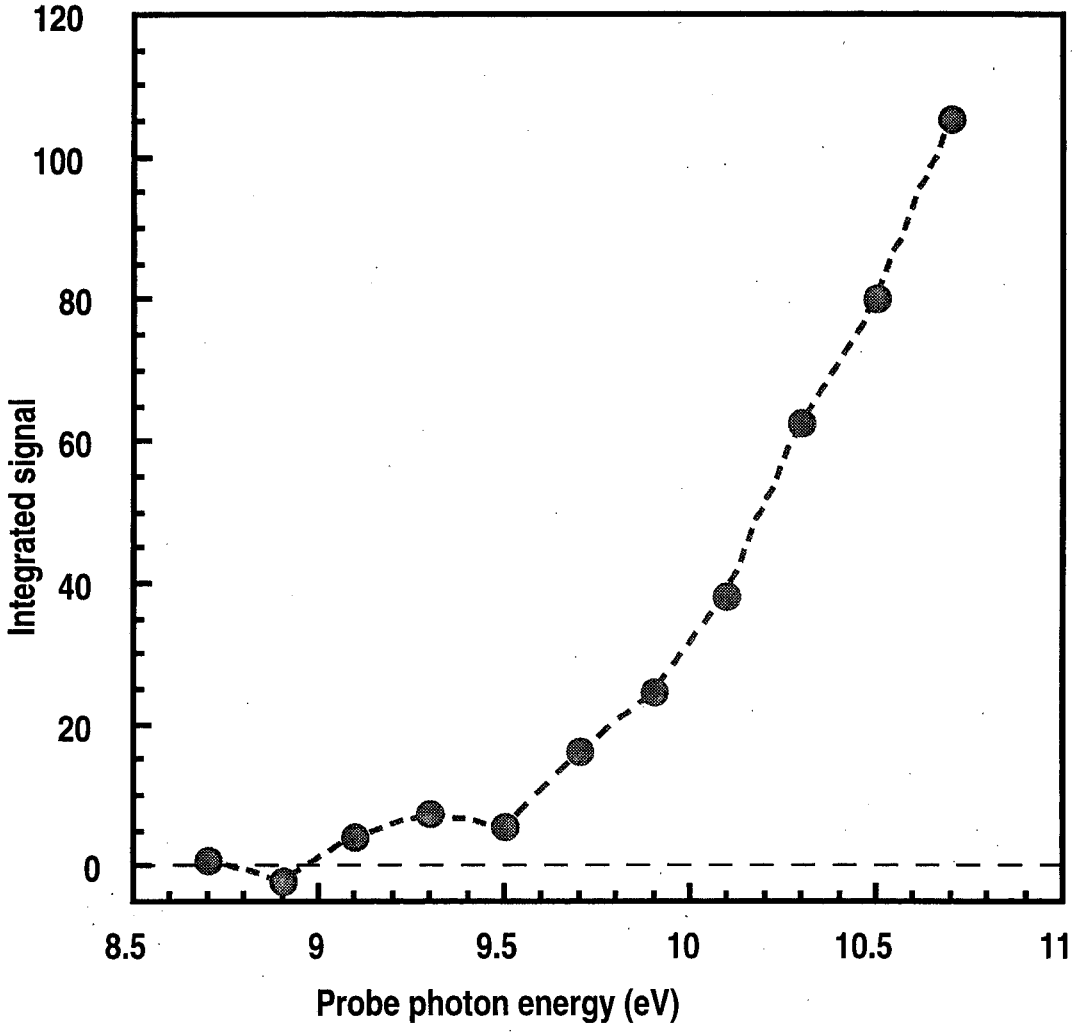
120
100
80
60
40
20
0
Integrated signal
8.5
9
9.5
10
10.5
11
Probe photon energy (eV)

Fig 10

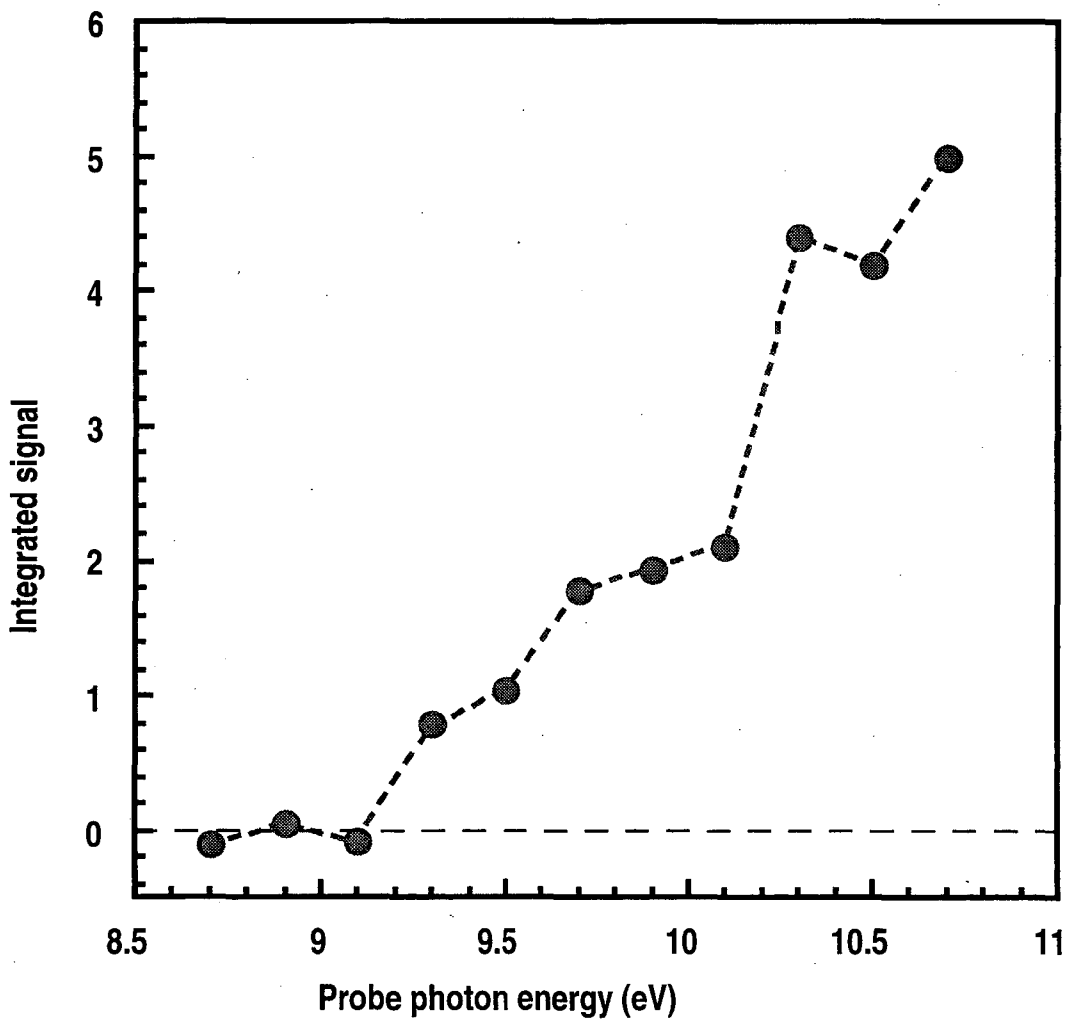
Integrated signal
6
5
4
3
2
1
0
8.5
9
9.5
10
10.5
11
Probe photon energy (eV)

Fig 11

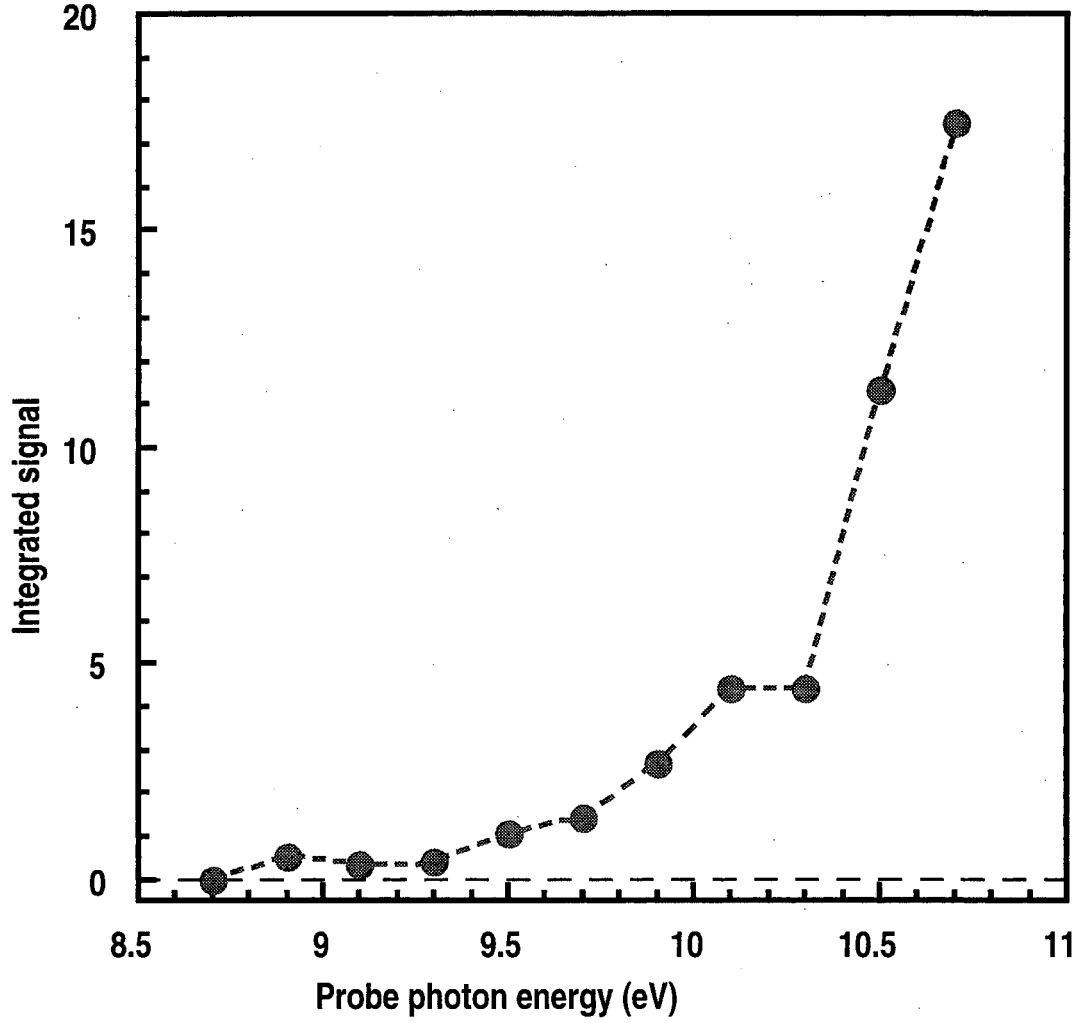
20
15
10
5
0
Integrated signal
8.5
9
9.5
10
10.5
11
Probe photon energy (eV)

Fig 12

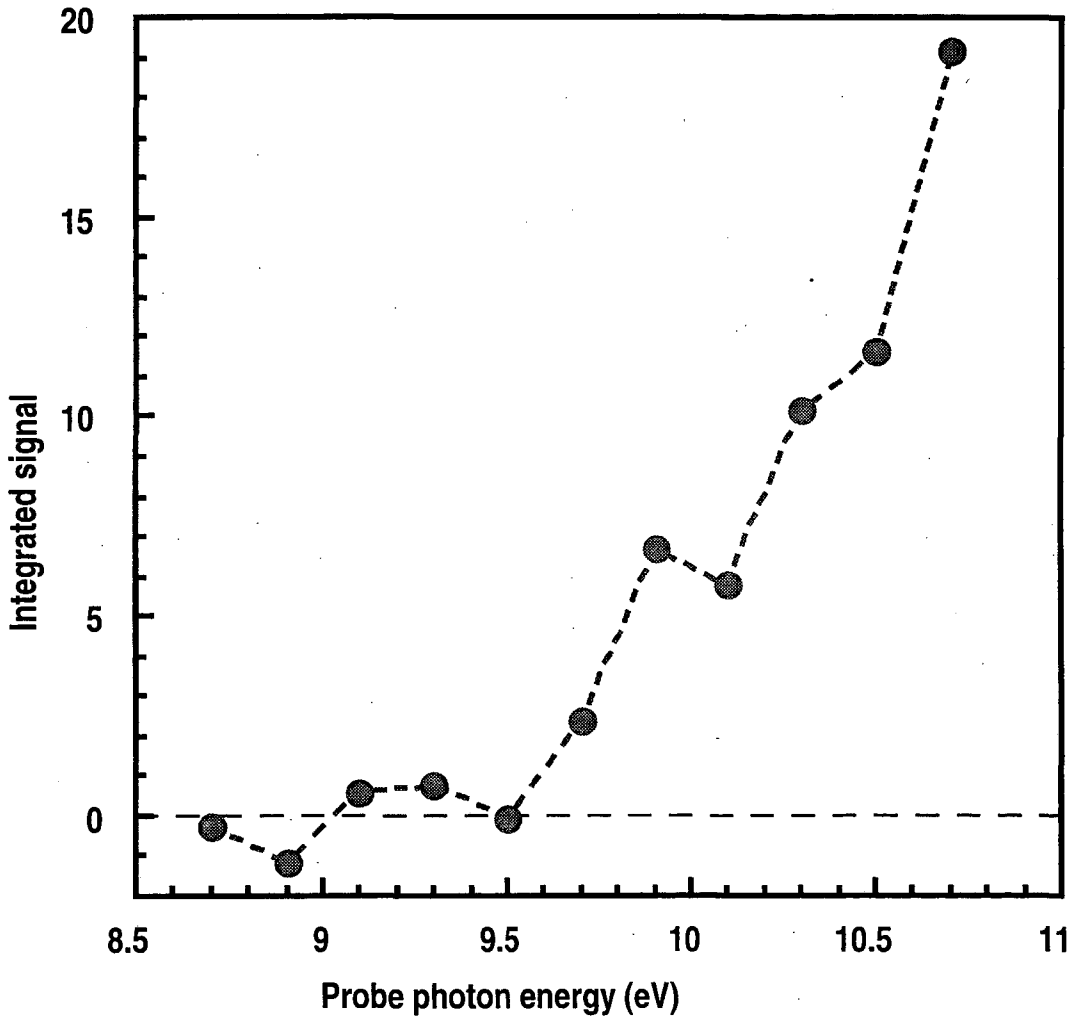
20
15
10
5
0
Integrated signal
8.5
9
9.5
10
10.5
11
Probe photon energy (eV)

Fig 13

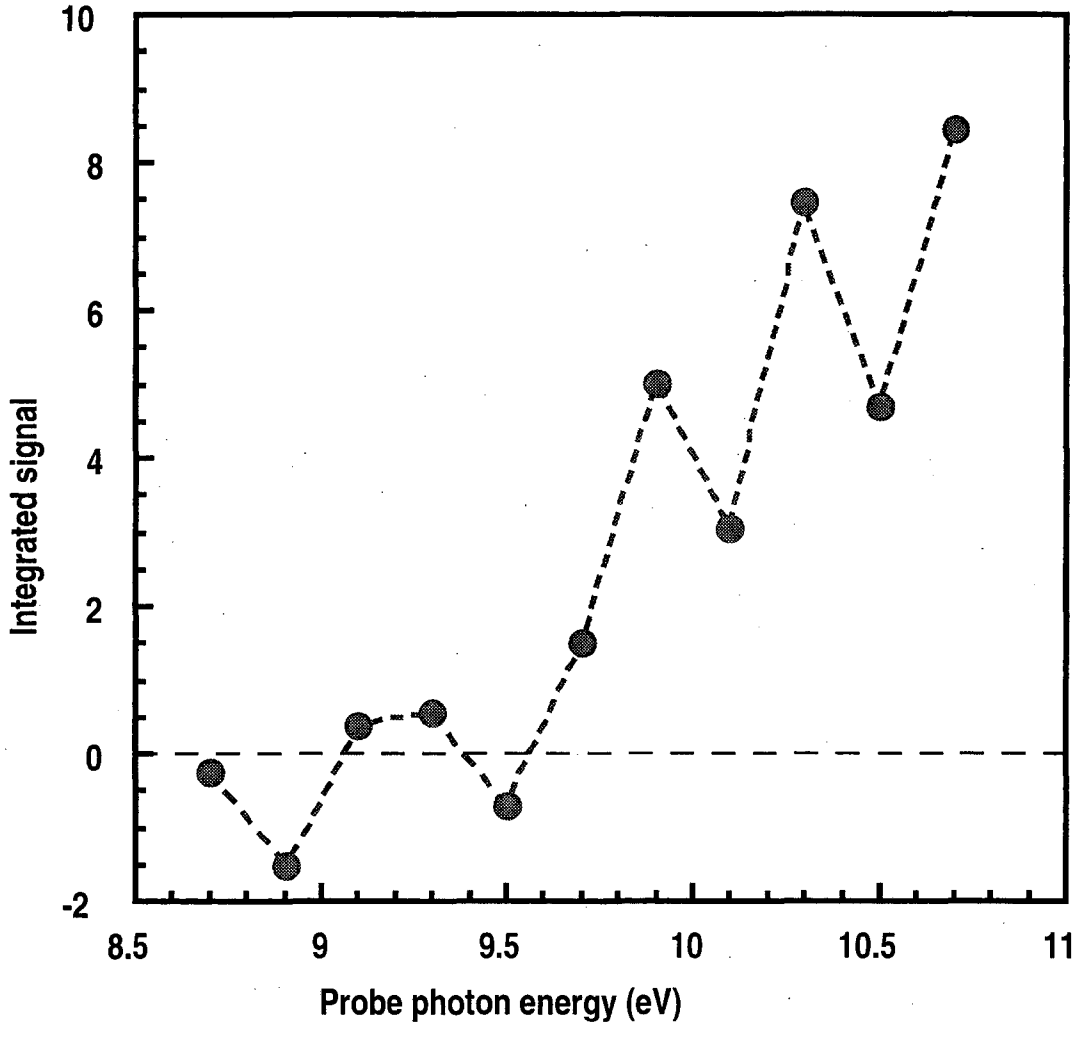
10
8
6
4
2
0
-2
Integrated signal
8.5
9
9.5
10
10.5
11
Probe photon energy (eV)

Fig 14

Ernest Orlando Lawrence Berkeley National Laboratory
One Cyclotron Road | Berkeley, California 94720

Prepared for the U.S. Department of Energy under Contract No. DE-AC03-76SF00098